Fakultät für Medizin

TranslaTUM, Klinikum rechts der Isar

Technische Universität München

The role of PDK1 in PI3K-driven intestinal carcinogenesis

Meng Lei

Vollständiger Abdruck der von der Fakultät für Medizin der Technischen Universität München zur Erlangung des akademischen Grades eines

Doktors der Medizin

genehmigten Dissertation.

Vorsitzender: Prof. Dr. Gabriele Multhoff

Prüfer der Dissertation:

1. **Prof. Dr. Dieter Saur**

2. **Prof. Dr. Radu Roland Rad**

Die Dissertation wurde am ……14.10.2020……. bei der Fakultät für Medizin der Technischen Universität München eingereicht und durch die Fakultät für Medizin am ……16.03.2021…… angenommen.

List of Contents

List of Tables

List of Figures

List of abbreviations

°C	degree Celsius
3D	three-dimensional
AB	alcian blue
AF	aelle frequency
AMP	adenosine monophosphate
ATP	adenosine triphosphate
AMN	appendiceal mucinous neoplasm
Apc	adenomatous polyposis coli
AKT	protein kinase B
AGC	protein kinase A, G, and C families
BrdU	bromodeoxyuridine / 5-bromo-2'-deoxyuridine
BRAF	V-Raf murine sarcoma viral oncogene homolog B
bp	base pair
BSA	bovine serum albumin
Chr	chromosome
CNV	copy number variation
CRC	colorectal cancer
CO_2	carbon dioxide
CIMP	the CpG island methylator phenotype
DNA	deoxyribonucleic acid
DMSO	dimethylsulfoxide
DNP	double nucleotide polymorphisml
DTT	dithiothreitol
DMEM	Dulbecco´s modified Eagle medium
DDR	DNA damage response
Da	Dalton

E2F	The E2 factor family
EtOH	ethanol
EDTA	ethylenediaminetetraacetic acid
EGF	epidermal growth factor
ERK	extracellular signal-regulated kinase
FAP	familial adenomatous polyposis
FITC	fluorescein isothiocyanate
FCS	fetal calf serum
FDR	false discovery rate
GA	gene name
GEMMs	genetically engineered mouse models
GAB1	GRB2 -associated-binding protein 1
GRB2	Growth factor receptor-bound protein 2
GAP	GTPase-accelerating protein
GFP	the green fluorescent protein
GEF	guanine nucleotide exchange factor
GTP	guanosine-5'-triphosphate
GSK	glycogen synthase kinase
GPCR	G protein-coupled receptor
g	gram
h	hour
H&E	hematoxylin and eosin
H_2O_2	hydrogen peroxide
H_2O	water
HNPCC	hereditary non-polyposis colorectal cancer
HPs	hyperplastic polyps
Hsp90	heat shock protein 90
IgG	immunoglobulin G
IEC	intestinal epithelial cells

IGF1	insulin-like growth factor 1
IRS	insulin receptor substrate-1
IN	intraepithelial neoplasia
IHC	immunohistochemistry
IMP	inosine 5'-monophosphate
kb	kilo base pair
KO	knock-out
Kras	v-Ki-ras2 Kirsten rat sarcoma viral oncogene homolog
KEGG	Kyoto encyclopedia of genes and genomes
LcWGS	Low coverage whole genome sequencing
LI	large intestine
LSL	*loxP*-stop-*loxP*
M	molar
mg	milligram
min	minute
mL	milliliter
mm	millimeter
mM	millimolar
MAPK	mitogen-activated protein kinase
mRNA	messenger ribonucleic acid
mTOR	mammalian target of rapamycin
MEK	MAPK/ERK kinase
MRCKα	myotonic dystrophy kinase–related CDC42-binding kinase alpha
MSI-H	high-level microsatellite instability
Mut	mutant
nm	nanometer
nM	nanomolar
NaCl	sodium chloride
NaOH	sodium hydroxide

NFKB	nuclear factor kappa-light-chain-enhancer of activated B cells
P53	transformation related protein 53
PIK3CA	phosphatidylinositol-4,5-bisphosphate 3-kinase catalytic subunit Alpha
PARP	ADP-ribose polymerase
PAK	the p21-activated kinases
PRK2	protein kinase C-related kinase–2
PKC	protein kinase C
PIF	a hydrophobic pocket in the kinase domain of Pdk1
pH	a numerical measure of the acidity or alkalinity of a solution
PBS	phosphate buffered saline
PCR	polymerase chain reaction
PDAC	pancreatic ductal adenocarcinoma
PDK1	3-phosphoinositide-dependent protein kinase 1
PH	pleckstrin homology
PI3K	phosphoinositide 3-kinase
PIP_2	phosphatidylinositol 4,5-bisphosphate
PIP_3	phosphatidylinositol 3,4,5-trisphosphate
PTEN	phosphatase and tensin homolog
Pik3r1	phosphoinositide 3 kinase regulatory subunit 1
PLCγ1	phosphoinositide phospholipase C gamma 1
PLK1	polo-like kinase 1
qRT-PCR	quantitative real time PCR
PCA	principle component analysis
p110α	a class I PI3K catalytic subunit
R26	*Rosa26*
Raf	proto-oncogene serine/threonine-protein kinase
RC	read covergae
RSK	ribosomal s6 kinase
RICTOR	rapamycin-insensitive companion of mammalian target of rapamycin

RNA	ribonucleic acid
rpm	revolutions per minute
rRNA	ribosomal ribonucleic acid
RT	room temperature
RTK	receptor tyrosine kinase
ST	mutation start position
SNP	single nucleotide polymorphism
Sufu	negative regulator of Hedgehog signaling
S6K1	ribosomal protein S6 kinase beta-1
SEM	standard error of mean
SD	standard deviation
SDS	sodium dodecyl sulphate
Smad	mothers against decapentaplegic homolog
SHP2	Src homology 2 (SH2) domains of SH2-containing phosphatase 2
SOS	Rac guanine nucleotide exchange factor
SSA	sessile serrated adenoma
SI	small intestine
SGK	serum/glucocorticoid regulated kinase 1
Seq	sequence
TLR	Toll-like receptor
TAE	tris-acetate-EDTA
TSA	traditional serrated adenoma
TSC	tuberous sclerosis complex
TKI	EGFR tyrosine kinase inhibitors
TAM	4-hydroxytamoxifen
TNF	tumor necrosis factor
TGF-β	transforming growth factor beta
tdTomato	a basic (constitutively fluorescent) orange fluorescent protein
TEC	tyrosine-protein kinase Tec

TRAF	tumor necrosis factor receptor-associated factor
TBK1	TANK(TRAF family member associated NFKB activator)-binding kinase 1
TSR	thrombospondin type 1 repeat
U	unit of enzyme activity
Vil	Villin
V	volt
VC	variant classification
VP	variant type
WES	whole exome sequencing
WT	wild type
µg	microgram
µL	microliter
µm	micrometer
µM	micromolar

1. Abstract

Serrated colorectal cancer is driven by oncogenic activation of *Kras*^{G12D} and/or *Braf*^{V637E} and/or *Pik3ca*^{H1047R}, and possibly others. Largely remains ambiguous for *Pik3ca* and its point mutation H1047R in a catalytic domain and how this mutation and its downstream effector PDK1 lead to the development of intestinal cancer. Thus, we generated mice with conditional activation of *Pik3ca*$^{H1047R/+}$ and/or inactivation of *Pdk1* in intestinal epithelial cells (IEC) using a Cre recombinase driven by the IEC-specific promoter *Villin*.

Based on previous research in our lab, most of the *Pik3ca*$^{H1047R/+}$ mice formed adenoma/adenocarcinoma in the small intestine (SI) and transcriptomic analysis of intestinal tissue of *Pik3ca*$^{H1047R/+}$ mice showed different tissue-specific signaling alterations that activated PI3K/AKT and decreased Wnt signaling were found in both the SI and LI(large intestine) while MAPK signaling was only increased the LI. Notably, Wnt and Hippo signaling was upregulated in duodenum tumor organoids from *Pik3ca*$^{H1047R/+}$ mice. These data indicate oncogenic *Pik3ca* is a driver gene for SI tumorigenesis and triggers a stepwise accumulation of genetic alterations. To address the role of PI3K downstream effector PDK1, we established the *Pik3ca*$^{H1047R/+}$, *Pdk1*$^{fl/fl}$ mouse line, and these mice develop cystic adenoma/mucinous adenocarcinoma exclusively in the LI. This observation suggests that the ablation of *Pdk1* with oncogenic *Pik3ca*$^{H1047R/+}$ in mice converts anatomical location of tumors from SI to LI. Thus, we postulate that *Pdk1* may play a dual role in the intestine, functioning as an oncogene in the SI and tumor suppressor in the LI. Transcriptomic analysis of intestinal tissue of *Pik3ca*$^{H1047R/+}$, *Pdk1*$^{fl/fl}$ mice showed increased MAPK, Wnt, and glycolysis in the SI and increased MAPK signaling and several metabolism pathways in the LI. To determine whether aberrant signaling expression levels are a result of an intrinsic signaling cascade or the extrinsic microenvironment arising from *Pdk1* ablation, and the role of *Pdk1* in intestinal tumorigenesis, we generated the *Pdk1*$^{fl/fl}$ mice model only

to eliminate Pdk1. The *Pdk1*$^{fl/fl}$ mice model exhibited lower body weight and shortened survival than the wild-type mice, also developed neoplasms in the LI. *In vitro* organoids derived from *Pdk1*$^{fl/fl}$ mice exhibited a stunted growth, and organoids isolated from *CreER*^{T2}, *Pdk1*$^{fl/fl}$ mice were resistant to *Pdk1* deletion by tamoxifen treatment *in vitro*. Metabolic analyses *in vivo* showed that *Pdk1* acts has a vital role in regulating the metabolism as well as proliferation, at least partially via intestinal barrier dysfunction. The MAPK signaling cascade activation only was confirmed *in vivo*, demonstrating the intestinal microenvironment is more critical for aberrant increased MAPK signaling in *Pik3ca*$^{H1047R/+}$, *Pdk1*$^{fl/fl}$ mice.

2. Zusammenfassung

Ein serratiertes kolorektales Karzinom wird die durch die Aktivierung eines oder mehrerer Onkogene ausgelöst, darunter besfinden sich K*ras*^{G12D}, *Braf*^{V637E}, *Pik3ca*^{H1047R} sowie möglicherweise andere Omkogene. Für *Pik3ca* und seine Punktmutation H1047R in einer katalytischen Domäne bleibt weitgehend unklar, wie diese Mutation zur Entwicklung von Darmkrebs führt. Es wurden Mäuse mit einer bedingten Aktivierung von *Pik3ca*$^{H1047R/+}$ und bzw. oder einer Deletion von *Pdk1* in den Darmepithelzellen (IEC) untersucht. Die Aktivierung erfolgte durch Cre-Rekombinase gesteuert durch den spezifischen Promotor Villin.

Die meisten *Pik3ca*$^{H1047R/+}$ -Mäuse bildeten im Dünndarm (small intestine, SI) ein Adenom bzw. Adenokarzinom. Die transkriptomische Analyse des Darmgewebes von *Pik3ca*$^{H1047R/+}$ -Mäusen zeigte verschiedene gewebespezifische Veränderungen der Signalübertragungswege. Die Aktivierung von PI3K / AKT und die Reduzierung der Wnt-Signalübertragung wurden sowohl im Dünn- als auch im Dickdarm (large intestine, LI) detektiert, während die MAPK-Signale sich nur im Dickdarm erhöhten. Insbesondere wurde die Wnt- und Hippo-Signalübertragung in Duodenum-Tumor-Organoiden aus *Pik3ca*$^{H1047R/+}$ -Mäusen hochreguliert. Diese Daten indizierten, dass das onkogene Pik3ca ein Driver-Gen für die SI-Tumorentstehung ist und eine graduelle Akkumulation genetischer Veränderungen auslöst. Um die Rolle des PI3K-Downstream-Effector PDK1 zu untersuchen, haben wir eine Mauslinie mit *Pik3ca*$^{H1047R/+}$ und *Pdk1*$^{fl/fl}$ etabliert. Diese Mäuse entwickeln ausschließlich im Dickdarm ein zystisches Adenom und bzw. oder muzinöses Adenokarzinom. Diese Beobachtung legt nahe, dass die Deletion von *Pdk1* zusammen mit der Mutation von onkogenem *Pik3ca*$^{H1047R/+}$ bei Mäusen die Entstehung von Tumoren im Dick- statt im Dünndarm auslöst. Wir postulieren daher, dass PDK1 im Darm eine doppelte Rolle spielt und als Onkogen im Dünndarm und als Tumorsuppressor im Dickdarm fungiert.

Die transkriptomische Analyse des Darmgewebes von *Pik3ca*$^{H1047R/+}$,*Pdk1*$^{fl/fl}$-Mäusen zeigte eine erhöhte MAPK, Wnt und Glykolyse im Dünndarm sowie eine erhöhte MAPK-Signalübertragung and mehrere Stoffwechselwege im Dickdarm. Um festzustellen, ob abweichende Signalspiegel das Ergebnis einer intrinsischen Signalkaskade oder einer extrinsischen Mikroumgebung sind, die sich aus der *Pdk1*-Ablation ergibt, sowie um die Rolle von PDK1 bei der intestinalen Tumorentstehung zu bestimmen, wurde das *Pdk1*$^{fl/fl}$-Mäusemodell nur zur Eliminierung von PDK1 generiert. *Pdk1*$^{fl/fl}$-Mäuse zeigten ein geringeres Körpergewicht und eine verkürzte Lebenserwartung als die Wildtyp-Mäuse, die ebenfalls Neoplasmen im Dickdarm entwickelten. *In vitro* Organoide, die von *Pdk1*$^{fl/fl}$-Mäusen stammen, zeigten ein verkümmertes Wachstum. Organoide, die aus *CreER*^{T2},*Pdk1*$^{fl/fl}$-Mäusen isoliert wurden, waren resitent gegen die durch eine Tamoxifen-Behandlung ausgelöste *Pdk1*-Deletion. Stoffwechselanalysen *in vivo* ergaben, dass PDK1 eine wichtige Rolle bei der Regulierung der Zell-Proliferation und des Metabolismus spielt. Das liegt zumindest teilweise darin begründet, dass die Funktion der Darmbarriere gestört wird. Die Aktivierung der MAPK-Signalkaskade wurde nur *in vivo* bestätigt, was darauf hindeutet, dass die Darmmikroumgebung für abweichend erhöhte MAPK-Signalwege in *Pik3ca*$^{H1047R/+}$,*Pdk1*$^{fl/fl}$-Mäusen entscheidend ist.

3. Introduction

3.1. Colorectal cancer

Colorectal cancer (CRC) is one of most lethal cancer types all over the world, affecting over 1.2 million patients and leading to more than 6,000,000 deaths each year (Siegel et al., 2020). The average 5-year survival of CRC patients is between approximately 50% to 65% and is highly related to clinical diagnosis stages (Brouwer et al., 2018). Gender and age, genetic susceptibility, unhealthy dietary intake, smoking, alcohol abuse, obesity, and environmental factors are all identified as possible etiological factors of colorectal cancer (Testa, Pelosi, & Castelli, 2018). Approximately 3% to 5% of CRCs are inherited, classified as familial adenomatous polyposis (FAP) and hereditary non-polyposis colorectal cancer (HNPCC) (Half, Bercovich, & Rozen, 2009; Leoz, Carballal, Moreira, Ocana, & Balaguer, 2015). The clinical stage of colorectal cancer accounts for the depth of local invasion (T stage), lymph node metastasis (M stage), and distant organ metastasis (N stage) (Kuipers et al., 2015). Stage assignment provides a standard diagnostic system for further treatment options. With the multidisciplinary collaboration of clinical departments, clinical treatment approaches on colorectal cancer patients mainly include surgical resection, chemotherapy, and radiotherapy (Xie, Chen, & Fang, 2020). Resection surgery remains the best choice for all stage I and some stage II patients (Bray et al., 2018). Short-term radiotherapy usually is applied to achieve better surgical outcomes. Recently some clinical trials have demonstrated the adjuvant chemotherapy of capecitabine, and oxaliplatin plus fluorouracil improves disease-free survival and overall survival of CRC stage III patients (Chang & Abbruzzese, 2005; Kemmochi et al., 2013; Petrioli et al., 2018).

3.2. Colorectal cancer progression model cancer

Understanding the cellular hierarchical and molecular mechanism of CRC progression

is of great importance for targeted-drug therapy and identifying novel markers to achieve an early-stage diagnosis and better clinical outcomes. CRC initiation and development are driven by a stepwise cumulation of genetic alterations (Armaghany, Wilson, Chu, & Mills, 2012; Danese et al., 2015; Hong, 2018; Rad et al., 2013; Wang et al., 2020). Atypical neoplastic precursor lesions of adenocarcinoma are reported as the most common precursor of human CRC malignancy, and this adenoma-carcinoma development sequence usually requires 5 to 15 years (Patil, Shadrach, Rybicki, Leach, & Pai, 2012). Over 70% of human neoplastic precursor lesions are accompanied by loss of the tumor suppressor *APC* coli (adenomatous polyposis), indicating *APC* genetic alterations are closely connected with CRC carcinogenesis (Stastna, Janeckova, Hrckulak, Kriz, & Korinek, 2019). In addition, oncogenic *BRAF* (V-Raf murine sarcoma viral oncogene homolog B) activation and/or loss of tumor suppressor *P53* (transformation related protein 53) due to variations in chromosome structure and copy number are also involved in the adenoma-carcinoma development sequence (Calistri et al., 2006). In another type of CRC progession model, the serrated polyp, has been evaluated a potential neoplastic lesion with the major histologic features of the saw-toothed and/or serrated infolding of the crypt epithelial layer (Yamane, Scapulatempo-Neto, Reis, & Guimaraes, 2014). WHO classified serrated polyps as sessile serrated adenomas (SSA), hyperplastic polyp (HP), and traditional serrated adenomas (TSA) (Crockett & Nagtegaal, 2019). Up to 30% of colorectal cancer has been estimated to evolve from precursor lesions via a ‘serrated progression pathway’ (De Palma et al., 2019) .The serrated polyps are considered not only to differ morphologically but also in genetic characters from ‘classic’ tumors, which arise through the adenoma-carcinoma sequence. Serrated polyps mainly have mutations in either *BRAF* and/or *PIK3CA* but less commonly in *APC (Borowsky et al., 2018)*. Typically, intraepithelial neoplasia (IN) is not found in serrated polyps but often exhibits MSI-H (high-level microsatellite instability) and CIMP-H (high methylation of CpG islands) (Yamane et al., 2014). While the genetic underpinning of *BRAF* and *BRAF*-driven CRC is quite well understood, little is known about *PIK3CA* and its point

mutation H1047R (*PIK3CA*^{H1047R}) and how this mutation leads to the development of intestinal cancer.

3.3. Oncogenic *Pik3ca*

The *Pik3ca* gene in mice offers paths for producing the p110 alpha protein (p110α), which is a subunit of one kinase called PI3K (phosphatidylinositol 3-kinase) (Yeates, Gallegos, Kozikowski, & Powis, 1999). The p110α protein is a catalytic subunit and it is responsible for the function of PI3K, while the other subunit, a p85 regulatory subunit produced by a different gene called phosphoinositide 3 kinase regulatory subunit 1 (*Pik3r1*), regulates the enzyme's activity. *Pik3ca* has been implicated in carcinogenesis in several cancer types, for example, *Pik3ca* is the most frequent mutated gene in mammary malignance and for a long time has considered as an oncogene, with two main hotspots mutations, the 1047 kinase domain, and the 542/545 helical domain (Anderson et al., 2020; Hadac et al., 2015; Tzanikou et al., 2019).

PI3K are a group of heterodimeric lipid kinases characterized by their phosphorylation of the 3'OH of inositol ring of phospholipids to generate the second messenger called PIP3 (phosphatidylinositol 3,4,5-trisphosphate) (J. Zhang, Roberts, & Shivdasani, 2011). PIP3 and PIP2 (phosphatidylinositol 4,5-bisphosphate) are generated by PI3K at the inner side of the cell membrane once RPTK (receptor protein tyrosine kinases) is activated (Ziemba, Burke, Masson, Williams, & Falke, 2016). Phospholipids are translocated to the inner membrane after recruitment by AKT (protein kinase B), then are phosphorylated and recruited by PDK1 (3-phosphoinositide-dependent protein kinase 1), PDK2, mTOR (mammalian target of rapamycin) complex, and mTORC2(Dieterle et al., 2014). PI3K/AKT is responsible for regulating a span of cellular functions, such as proliferation and survival (Fruman et al., 2017). PI3K and its crosstalk with the AKT signaling and mTOR pathways is the issue of an immense body of study and progress, and PI3K inhibition has met with restricted achievement in recent clinical trials against cancer (Bian et al., 2018; Sathe et al., 2018; Shi et al., 2018). Although monotherapy of PI3K inhibition appears to be unsatisfactory in their

clinical potential, there is chance in optimizing PI3K inhibition as a supplement of combination therapies regimen with inhibition components including TKIs (EGFR tyrosine kinase inhibitors), MEK (MAPK/ERK kinase) inhibitors, PARP (ADP-ribose polymerase) inhibitors, and in breast cancer, aromatase inhibitors (Bian et al., 2018; E, Xing, Gong, He, & Zhang, 2015; H. Sato et al., 2018).

3.4. Phosphoinositide dependent kinase-1 (PDK1)

Phosphoinositide dependent kinase-1 (PDK1), one of the many downstream targets of PI3K products, is a PH (pleckstrin homology) domain-containing kinase that phosphorylates AKT isoforms and other AGC kinases family (protein kinase A, G, and C families) including S6K1 (ribosomal protein S6 kinase beta-1), p70S6K, SGK (serum/glucocorticoid regulated kinase 1), RSK (ribosomal s6 kinase), and the PKC (protein kinase C) family (Biondi et al., 2002; Mora, Komander, van Aalten, & Alessi, 2004). PDK1 is a ubiquitous signaling transducer in eukaryotes, the ablation of which is lethal in mammals (Lawlor et al., 2002). Death in a constitutive *Pdk1* knock-out mouse model occurred, on average, at embryonic day 9.5 due to phenotypic alterations and multiple organ developmental disorders.

PDK1 protein is medium-sized and globular with only two domains, a C-terminal PH domain, as well as an N-terminal kinase domain (Biondi et al., 2002; Komander et al., 2004). The C-terminal PH domain is to bind specifically with two products of PI3K, PIP3 and PIP2 (Kobayashi, Deak, Morrice, & Cohen, 1999). The PIF pocket domain is at the N-terminal lobe of the kinase domain, and it combines with a highly conserved phosphorylated motif, also called a hydrophobic motif, presented on many PDK1 substrates (Collins, Deak, Arthur, Armit, & Alessi, 2003). Phosphorylation of serine 241 is localized in the activating loop of PDK1 kinase region, which is affected by PDK1 catalysis in trans-phosphorylation and is crucial for kinase activity (Casamayor, Morrice, & Alessi, 1999). Phosphoinositides simultaneously bind PDK1 and AKT, not only facilitating the physical contact to make a conformational alteration but also increasing

the chances of AKT being phosphorylated by PDK1 on threonine 308 (Stokoe et al., 1997). PDK1-mediated phosphorylation is an essential step in activation of AKT, which is effectuated via the serine 473 phosphorylation intervened by mTORC2 (Sarbassov, Guertin, Ali, & Sabatini, 2005). PDK1 also has been reported to play roles in AGC kinase family phosphorylation and the phosphorylation of other kinases, such as p21-activated kinase (PAK), Rho-associated protein kinase 1 (ROCK1), polo-like kinase1, β3 integrin, and myotonic dystrophy kinase-related CDC42-binding kinase alpha (MRCKα), and other (di Blasio et al., 2015; Gagliardi et al., 2014; King et al., 2000; Tan et al., 2013).

PDK1 itself catalyzes the phosphorylation of the PDK1 activation loop serine 241, resulting that PDK1 is not easily accessed by other phosphatases and shows a low chance of activation by genetic mutation (Wick et al., 2003). Aberrant protein expression of PDK1 has been identified in a plethora of cancer types; for example, PDK1 protein is overexpressed in most breast neoplastic lesions and gastric carcinoma (Arsenic, 2014; Pal, Outram, & Basu, 2013).

Previously research in our lab indicated that *Pdk1* deletion could block *Pik3ca*-driven pancreatic carcinogenesis in the genetic mouse model (Eser et al., 2013). A logical continuation of this work is to assess the role of *Pdk1* in *Pik3ca*-driven colorectal carcinogenesis to address whether it has similar functions in different carcinogenesis contexts.

3.5. A *Pik3ca/Pdk1*-driven mouse model for colorectal cancer

PIK3CA mutations occur in nearly 20% to 30% of human CRC (Velho et al., 2008); however, its role in the CRC tumorigenesis has yet to be well defined. To elucidate its role, genetically engineered mouse models (GEMMs) with mutated *Pik3ca* have been generated to imitate human colorectal malignance (Hadac et al., 2015; Leystra et al., 2012). This model is based on a latent oncogenic knock-in *Pik3ca*^{H1047R} (coding

p110a^{H1047R}) site flanked by a lox-stop-lox (LSL) at Rosa26 site (Hingorani et al., 2003). To switch on the oncogenic *Pik3ca*^{H1047R} as well as PI3K/AKT signaling, especifically in the intestine, we utilized the well-established *Villin-Cre* promoter to instruct recombination only in intestinal epithelial cells (el Marjou et al., 2004). Cre was produced driven by a 9 kb (kilo base pair) regulatory region of the *Villin* gene. Generally, genetic recombination was originated in the visceral endoderm at embryonic day E9, and in the entire intestinal epithelium by E12.5, but not in other tissues. The expression of Cre was maintained all over the adulthood. In our study, *Villin-Cre*, *Pik3ca*^{H1047R} (include homozygous *Villin-Cre*, *Pik3ca*$^{H1047R/H1047R}$ and *Villin-Cre*, *Pik3ca*$^{H1047R/+}$ heterozygous mice) mice develop hyperplasia, advanced neoplasia as well as intestinal carcinoma, and over 20% of the mice tumors have been found to metastasize at other organs.

To decipher the PI3K downstream PDK1 effect on *Pik3ca*-driven colorectal cancer tumorigenesis, we ablated *Pdk1* only in the epithelium of the intestine by floxed *Pdk1* (Lawlor et al., 2002). In the *Pdk1*$^{fl/fl}$ line, exons 3 and 4 are silenced by loxP sites and then deleted by the Cre recombinase to abolish the autonomous expression of the PDK1. Furthermore, PDK1 interrelates with phosphoinositides via a pleckstrin homology (PH) domain. We established the *Pdk1*$^{K465E/fl}$ mouse line that contains a point mutation of exon 12 of the *Pdk1* gene (Bayascas et al., 2008). This mutation triggers a change in conformity in the PH domain of the *Pdk1* gene and thereby causes an inhibition of the binding of PDK1 to PIP3. However, PDK1 is expressed normally.

3.6. PI3K-PDK1 crosstalk

PI3K-AKT-mTORC1 and Ras-Raf-ERK (Raf represents proto-oncogene serine/threonine-protein kinase,ERK represents extracellular signal-regulated protein kinase) pathway integration has been investigated for more than 30 years, and in that time, several patterns of crosstalk have been revealed, including cross-activation, cross-inhibition, pathway convergence, and feedback loops (Mendoza, Er, & Blenis,

2011; Steelman et al., 2011).

The Ras-Raf-ERK pathway and PI3K-AKT-mTORC1 cross-activation signaling recruit PI3K, TSC2 (tuberous sclerosis complex 2), and mTOR complex 1. Ras-GTP directly combines and allosterically regulates PI3K (Castellano & Downward, 2011; Murillo et al., 2014; Wang et al., 2008). Besides, once the Ras-Raf-ERK pathway is strongly activated, it will upregulate mTORC1 activity via RSK and ERK to the TSC complex and ERK scaffolds link multiple signals of the mTORC1 pathway (Winter, Jefferson, & Kimball, 2011). The cross-inhibition between the Ras-Raf-ERK and PI3K-AKT-mTORC1 has been addressed in several studies. For instance, MEK inhibitors upregulate EGF (epidermal growth factor)-driven AKT activation (Turke et al., 2012). Cross-inhibition between Raf and AKT is initiated by strong IGF1 (insulin-like growth factor1) activation (R. Li, Pourpak, & Morris, 2009). The convergence of the Ras-Raf-ERK pathway and PI3K-AKT-mTORC1 pathway indicates that upon activated, RSK, AKT, ERK, and S6K often act on the identical substrate to promote cell metabolism, proliferation, survival, and motility (Chappell et al., 2011; Ye, Cai, Zheng, Evers, & She, 2014). For instance, ERK phosphorylates FOXO3A at Ser294, Ser344, and Ser425 to direct FOXO3A's proteasome-induced degradation (Yang et al., 2008). The phosphorylation of FOXO1 and FOXO3A mediated by AKT and SGK at Ser253, Ser315 and Thr32, is to preclude them from entering the nucleus and activating quiescence and apoptotic related gene expression programs (Brunet et al., 2001). The level of pathway activation strength and duration is adjusted by feedback loops and the intensity of the stimulus. The agonists related to Ras-Raf-ERK activation intersect only partially with signals to PI3K-AKT-mTORC1. One paradigm is insulin and insulin growth factor 1 (IGF1), which are mild Ras-Raf-ERK signaling activators, but strong PI3K-AKT-mTORC1 signaling activators (Schlessinger, 2000; Zheng & Quirion, 2006). In addition, signaling dynamics are usually regulated by positive feedforward loops and negative feedback loops, which crosstalk modes also are existed in both the Ras-Raf-ERK and PI3K-AKT-mTORC1 signaling. A positive loop engaged GAB (growth factor

receptor-bound protein 2 associated-binding protein 1) that can connect with RasGAP (Ras GTPase-activating proteins), SHP2 (Src homology 2 domains of SH2-containing phosphatase 2), PIP3, and PI3K (Agazie & Hayman, 2003; Montagner et al., 2005). SHP2 reduces phosphorylation of the RasGAP on GAB1 and its bound RTKs, thus inhibiting Ras inactivation and enlarging Ras-ERK signaling. Furthermore, GAB1 recruitment of PI3K produces local PIP3, which attracts additional GAB1 synthesis to the membrane and then activates PI3K pathway (S. Q. Zhang et al., 2002). By contrast, for example, negative feedback loops such as that of ERK phosphorylates and reduces SOS (Rac guanine nucleotide exchange factor), Raf, and MEK1, further decreasing activation of ERK (Lemmon & Schlessinger, 2010; Schlessinger, 2000). ERK also triggers the synthesis of genes encoding sprouty proteins involving in Raf-induced MEK activation and MAPK (mitogen-activated protein kinase) phosphatase residues, which inhibit ERK (Ebisuya, Kondoh, & Nishida, 2005). In addition, the negative feedback loop of PI3K-AKT-mTORC1 recruit S6K phosphorylation of IRS (insulin receptor substrate-1) and RICTOR (rapamycin insensitive companion of mammalian target of rapamycin), which inhibit AKT activity and mTORC1 signaling (Luo, Field, Lee, Engelman, & Cantley, 2005; Manning, 2004).

3.7. Aim of the work

Previous research in our lab showed that the PI3K/ PDK1 pathway is vital for PDAC (pancreatic ductal adenocarcinoma) initiation and that inactivation of *Pdk1* could inhibit *Pik3ca*-driven PDAC in mice. As a continuation of that work, we seek to reveal whether *Pdk1* plays a similar role in intestinal carcinogenesis through Cre-based GEMM of CRC and determine the role of *Pik3ca* and *Pdk1* for tumor initiation and progression (Eser et al., 2013). Therefore, the 1) *Villin-Cre, Pik3ca*$^{H1047R/+}$; 2) *Villin-Cre, Pik3ca*$^{H1047R/+}$*, Pdk1*$^{fl/fl}$, 3) *Villin-Cre, Pik3ca*$^{H1047R/+}$*, Pdk1*$^{K465E/fl}$, and 4) *Villin-Cre; Pdk1*$^{fl/fl}$ mouse models were employed, which allow for activation of *Pik3ca* and/or deletion of *Pdk1* in intestinal epithelial cells *in vivo*. First, we measured the survival and metastasis

of the mice model and quantified intestinal hyplersia/adenoma/carcinoma lesions. Second, the signaling and metabolism alterations were detected by IHC (immunohistochemistry) and metabolism assays. Besides, mouse-derived organoids biobank were established for *in vitro* studies. The effect of oncogenic *Pik3ca* and/or *Pdk1* deletion on growth and proliferation were evaluated, and downstream effectors and possiable mechanisms were explored by RNA sequencing.

4. Materials

4.1. Enzymes and reagents

Table 1. Enzymes and reagents

Enzymes and reagents	Source
Agarose	Sigma-Aldrich Productions GmbH, Germany
Ammonium persulfate ($(NH4)_2SO_4$)	Sigma-Aldrich Productions GmbH, Germany
Ampicillin sodium salt	Carl Roth GmbH, Baden-Württemberg
Dimethylsulfoxide (DMSO)	Carl Roth GmbH, Karlsruhe
Dodecylsulfate Na-salt in pellets (SDS)	Serva Electrophoresis GmbH, Heidelberg
Dulbecco's phosphate buffered saline	Biochrom AG, Germany
Ethanol	Merck Group (Merck KGaA), Germany
Ethidium bromide	Sigma-Aldrich Productions GmbH, Germany
Ethylenediaminetetraacetic acid (EDTA)	Sigma-Aldrich Productions GmbH, Germany
GeneRuler™ 100bp DNA ladder	Fermentas GmbH, Germany
Glycerol	Sigma-Aldrich Productions GmbH, Germany
Glycin Pufferan®	Carl Roth GmbH, Germany
HEPES Pufferan®	Carl Roth GmbH, Germany
Histosec® pastilles	Merck Group (Merck KGaA), Darmstadt
HotStarTaq DNA polymerase	Qiagen GmbH, Hilden
Hydrochloric acid (HCl)	Merck Group (Merck KGaA), Darmstadt
Methanol	Merck Group (Merck KGaA), Darmstadt
Nonidet P40	*Roche* GmbH, Germany
Proteinase K	Roche GmbH, Germany
Rnase-free Dnase	Qiagen GmbH, Germany
RnaseA	Fermentas GmbH, Germany
Rotiphorese® gel 30	Carl Roth GmbH, Germany

Sodium acetate buffer solution	Sigma-Aldrich Productions GmbH, Germany
Sodium chloride (NaCl)	Merck Group (Merck KGaA), Darmstadt
Sodium hydroxide solution (NaOH)	Merck Group (Merck KGaA), Darmstadt
Tamoxifen	Sigma-Aldrich Productions GmbH, Germany
TE buffer, pH 8.0	AppliChem GmbH, Darmstadt
TEMED	Carl Roth GmbH, Karlsruhe
Triton® X-100	Merck Group (Merck KGaA), Darmstadt
Tween® 20	Carl Roth GmbH, Germany
1 kb DNA extension ladder	Invitrogen GmbH, Karlsruhe
1,4-Dithiothreitol (DTT)	Carl Roth GmbH, Germany
2-Log DNA ladder	New England Biolabs GmbH, Germany
2-Mercaptoethanol	Sigma-Aldrich Productions GmbH, Germany
2-Propanol	Carl Roth GmbH, Karlsruhe

4.2. Antibodies

Table 2. Primary and secondary antibodies

Antibody	**Source**
Ki67 (SP6), #Ki68ic0i	Innovative Diagnostik-Systeme Dr. Christian Sartori GmbH & Co. KG
p-p44/42 MAPK (T202/T204), #4695	Cell Signaling Technology, Inc., USA

4.3. Molecular biology

Table 3. Kits used for molecular biology

Kits	**Source**
QIAamp DNA mini kit	Qiagen GmbH, Hilden
QIAshredder	Qiagen GmbH, Hilden
Rneasy mini kit	Qiagen GmbH, Hilden

TruSeq® Stranded mRNA (messenger ribonucleic acid) kit	Illumina, San Diego, CA, USA

All buffers were prepared by using dH2O.

Table 4. Buffers

Buffers	Components
50x TAE buffer, pH 8.5	5.71% Acetic acid 2 M Tris 50 mM EDTA
Protein lysis buffer, pH 7.9	Phosphatase inhibitor Protease inhibitor 0.5% Nonidet P40 10% Glycerol 1 mM EDTA 50 mM HEPES 150 mM NaCl
PCR Soriano lysis buffer	0.5% Triton® X-100 1% 2-Mercaptoethanol 1x Gitschier's buffer 400 µg/mL Proteinase K (prepare prior to use)
SucRot solution (PCR)	30% Saccharose 1.5 mg/mL Cresol red 100 mM Tris(pH 9.0)

4.4. Primers

Oligonucleotides were made by Eurofins MWG and then dissolved in H_2O for further use to 10 µM concentration.

Table 5. Primers

PCR name	Primer name	Sequence (5´ → 3´)
$CreER^{T2}$	$CreER^{T2}$ forward	GAATGTGCCTGGCTAGAGATC
	$CreER^{T2}$ reverse	GCAGATTCATCATGCGGA
	$CreER^{T2}$ recombined	CGATCCCTGAACATGTCCATC

	reverse	
LSL-Pik3ca^{H1047R}	Pik3ca^{H1047R} forward	TGAATAGTTAATTGGAGCGGCCGCAATA
	Pik3ca^{H1047R} reverse	AAATAGCCGCAGGTCACAAAGTCTCCG
Pdk1$^{fl/fl}$	Pdk1 floxed forward	ATCCCAAGTTACTGAGTTGTGTTGGAAG
	Pdk1 floxed reverse	TGTGGACAAACAGCAATGAACATACACGC
Pdk1$^{fl/fl}$ recombination	Pdk1 recombined forward	CTATGCTGTGTTACTTCTTGGAGCACAG
	Pdk1 non-recombined forward	CCCTCTAGCAAATGTTCTGTCTGGAATGTCT
	Pdk1 floxed reverse	TGTGGACAAACAGCAATGAACATACACGC
Tva	Tva common forward	AAAGTCGCTCTGAGTTGTTAT
	Tva mut reverse	GCGAAGAGTTTGTCCTCAACC
	Tva wt reverse	GGAGCGGGAGAAATGGATATG
Villin^{Cre}	V-Cre1 forward	CAAATGTTGCTTGTCTGGTG
	V-Cre2 forward	GTCAGTCGAGTGCACAGTTT
	V-Cre1 reverse	GTGTGGGACAGAGAACAAACC
	V-Cre2 reverse	ACATCTTCAGGTTCTGCGGG
Pdk1^{K465E}	Pdk1^{K465E} forward	GGG TGA AGC ATG GAA TCT GTG TCT T
	Pdk1^{K465E} reverse	GCC AGG ATA CCT AAG AGT ACC TAG AA
Mycoplasma test	Forward 1	CGCCTGAGTAGTACGTTCGC
	Forward 2	CGCCTGAGTAGTACGTACGC
	Forward 3	TGCCTGGGTAGTACATTCGC
	Forward 4	TGCCTGAGTAGTACATTCGC
	Forward 5	CGCCTGAGTAGTATGCTCGC
	Forward 6	CACCTGAGTAGTATGCTCGC
	Forward 7	CGCCTGGGTAGTACATTCGC
	Reverse 1	GCGGTGTGTACAAGACCCGA
	Reverse 2	GCGGTGTGTACAAAACCCGA
	Reverse 3	GCGGTGTGTACAAACCCCGA

4.5. organoids culture

Table 6. Organoids culture media

Medium	**Components**
Organoid media	L-WRN medium Rock inhibitor (1:100)
Freezing medium	70% Advanced DMEM

	20% FBS 10% DMSO
L-WRN medium	Advanced DMEM 10% FCS 1% Penicillin–Streptomycin 1% Glutamine
L-WRN harvesting medium	Advanced DMEM 10% FBS 1% L-Glutamine 1% HEPES 1% Penicillin–Streptomycin

Table 7. Reagents for organoids culture and medium

Reagents / Kits	**Source**
Collagenase type 1	Gibco® Life Technologies, Darmstadt
Cell recovery solution	Corning MA, USA
Dulbecco's modified eagle medium with L-glutamine (DMEM)	Sigma-Aldrich® MO, USA
Dulbecco's phosphate buffered saline (PBS)	Sigma-Aldrich® MO, USA
Fetal calf serum (FCS)	Biochrom GmbH Berlin, Germany
HEPES	Sigma-Aldrich® MO, USA
L-Glutamine	Sigma-Aldrich® MO, USA
Matrigel®Matrix	Corning MA, USA
Penicillin/Streptomycin solution	Invitrogen GmbH, Karlsruhe
TrypLE	Gibco® Life Technologies, Darmstadt
Venor® mycoplasma detection kit	Minerva Biolabs GmbH, Berlin
Y-27632	Sigma Taufkirchen

4.6. Histology

Table 8. Buffers and solutions

Buffers	**Components**
Alcian blue (pH 2.5)	3% Acetic acid 1% Alcian blue

	dH_2O
Nuclear fast red	2.5% Aluminium sulphate 0.1% Nuclear fast red dH_2O

Table 9. Reagents for histological assays

Reagents / Kits	**Source**
Acetic acid (glacial)	Merck Group (Merck KGaA), Darmstadt
Alcian blue 8GX	Sigma-Aldrich® , Munich
Aluminium sulfate	Honeywell Specialty Chemicals GmbH, Seelze
Antigen unmasking solution	Vector Laboratories, Inc., USA
Avidin/biotin kit	Vector Laboratories, Inc., USA
Nuclear fast red	Merck Group (Merck KGaA), Darmstadt
DAB peroxidase substrate kit	Vector Laboratories, Inc., USA
Donkey serum D9663	Sigma-Aldrich® , Munich
Eosin solution	Waldeck GmbH, Münster
Goat serum G9023	Sigma-Aldrich® , Munich
Hematoxylin	Merck Group (Merck KGaA), Darmstadt
Hydrogen peroxide 30%	Merck Group (Merck KGaA), Darmstadt
Pertex mounting medium	MEDITE GmbH, Burgdorf
Roti® Histol	Carl Roth GmbH, Karlsruhe
Sucrose	Merck Group (Merck KGaA), Darmstadt
ABC kit	Vector Laboratories, Inc., Burlingame, USA

Table 10. Secondary antibodies

Antibody	**Source**
anti-goat IgG (H+L)	Vector Laboratories, Inc., Burlingame, CA, USA
anti-rabbit IgG (H+L)	Vector Laboratories, Inc., Burlingame, CA, USA

4.7. Technical equipment

Table 11. Technical equipment

Device	Source
Aperio Versa 8 Digital Scanner	Leica Microsystems
BiometraTone PCR machines	Analytic Jena AG
Bag sealer Folio FS 3602	Severin Elektrogeräte GmbH, Sundern
Centrifuge Z323K	HERMLE Labortechnik GmbH
CLARIOstar® platereader	BMG Labtech
CO2 incubator HERAcell® 160i	Thermo Fisher Scientific
CO2 incubator HERAcell® 250i	Thermo Fisher Scientific
Electrophoresis Power Supply EPS 601	Amersham Pharmacia Biotech
Electrophoresis Power Supply EV243	CONSORT – Topac Inc.
Electrophoresis power supply Power Pac 200	Bio-Rad Laboratories GmbH, Munich
ENVAIR eco safe comfort® biological safety cabinet	ENVAIR Ltd.
Gel tray SUNRISE™	Life Technologies
Gel trays Biometra Compact® L/XL	Biometra Analytik Jena Company
Glass ware, Schott Duran®	Schott AG
Grant JB Nova water bath	Grant Instruments
Heraeus™ Multifuge™ X3FR Centrifuge	Thermo Fisher Scientific
Heated paraffin embedding module EG1150 H	Leica Microsystems GmbH, Wetzlar
Horizontal gel electrophoresis system	Biozym Scientific GmbH, Hessisch Oldenburg
Hiseq2000 platform	Illumina, San Diego, CA, USA
Hiseq2500 platform	Illumina, San Diego, CA, USA
Lambda™ Plus Multi-Channel Pipettor	Corning Life Sciences
Leica DM500	Leica Microsystems
Leica Dmi8 Microscope	Leica Microsystems
Leica M205 FCA	Leica Microsystems
Magnetic stirrer Ikamag® REO	IKA® Werke GmbH & Co. KG

Magnetic stirrer MR 3000	Heidolph Instruments
Melag Oven	WMW AG
Microcentrifuge 5415 C	Eppendorf AG
Microcentrifuge 5415 D	Eppendorf AG
Microcentrifuge 5427 R	Eppendorf AG
Microscope Axiovert A1	Carl Zeiss AG
Microscope Camera Axiocam 503 mono	Carl Zeiss AG
Microscope Leica DFC3000G	Leica Camera AG
Microwave	Ok. – Mediamarkt
Minicentrifuge	Lab Logistics Group GmbH
Multi-Axle-Rotating-Mixer RM5	Ingenieurbüro CAT M. Zipperer GmbH
Multipette® E3	Eppendorf AG
Multipette®plus	Eppendorf AG
Nanophotometer	IMPLEN GmbH
Neubauer hemocytometer, improved	LO-Laboroptik GmbH
Pasteur pipettes	Hirschmann Laborgeräte GmbH & Co. KG,
Pipette Tips Axygen®	Corning Life Sciences
Pipettes Reference®, Research®, Research plus®	Eppendorf AG
Pipetus®	Hirschmann Laborgeräte GmbH & Co. KG,
Precision balance PCB	KERN & SOHN GmbH
Qubit® 2.0 Fluorometer	Invitrogen GmbH, Karlsruhe
Rotamax 120® orbital shaker	Heidolph Instruments
Surgical instruments	Thermo Fisher Scientific, Inc., Waltham, MA, USA
Stripettor™ Ultra Pipet Controller	Corning Life Sciences
Thermocycler Tone	Biometra GmbH
Thermomixer Comfort®	Eppendorf AG
ThermoQ® dry bath	Hangzhou Bioer Technology Co. Ltd
Uvsolo touch® imaging system	Analytic Jena AG
Vortex Genie 2	Scientific Industries, Inc.

4.8. Disposables

Table 12. Consumables

Disposable	Source
24 Well Cell Culture Plate	Corning Life Sciences, USA
Cell culture plastics	Greiner Bio-one GmbH,Solingen, Germany
Cell strainer, 100 µm, yellow	BD Biosciences, Franklin Lakes, NJ, USA
Combitips BioPur®	Eppendorf AG, Hamburg
Cellstar® falcon tubes 15ml, 50ml	Greiner Bio-one GmbH,Solingen, Germany
Cover slips	Gerhard Menzel, Glasbearbeitungswerk GmbH & Co. KG, Braunschweig
Cotton-tipped applicators	Lohmann & Rauscher GmbH & Co. KG, Neuwied
Disposable scalpels	Feather Safety Razor Co., Ltd., Osaka, Japan
Falcon cell strainer 70 µm and100 µm	Corning Life Sciences,NY, USA
Glass slides Superfrost® Plus	Gerhard Menzel, Glasbearbeitungswerk GmbH & Co. KG, Braunschweig
Microtome blades S35	Feather Safety Razor Co., Ltd., Osaka, Japan
MEDITE® coverglass	MEDITE GmbH, Burgdorf
Microplate, 96-well	F-Bottom Greiner Bio-one GmbH, Solingen, Germany
Multiply®-µStrip PCR reaction tubes	Sarstedt AG & Co., Nümbrecht
Reaction tubes, 0.5 ml, 1.5 ml and 2 ml	Eppendorf AG, Hamburg
Safe seal pipette tips	Biozym Scientific GmbH, Hessisch Oldenburg
Serological pipettes 2ml, 5ml, 10ml, 25ml	Greiner Bio-one GmbH Solingen, Germany
Superfrost Plus glass slides	Thermo Scientific, MI, USA
Tissue embedding cassette system	Medite GmbH, Burgdorf
Vectashield Vector	Laboratories Peterborough, UK

4.9. Software

Table 13. Software

Software	Source
AxioVision 4.8	Carl Zeiss, Oberkochen
Adobe illustrator	Adobe, USA
Endnote X9	Clarivate Analytics
ImageJ 1.52p	National Institutes of Health
ImageScope Ver 12.4.3.5008	Leica Microsystems CMS GmbH
GraphPad Prism 8	La Jolla, CA, USA
Leica Application Suite X 3.4.2.18368	Leica Microsystems CMS GmbH
Microsoft Office	Microsoft Corporation, Redmont
R studio(Version 1.3.959)	© 2009-2020 RStudio, PBC

5. Methods

5.1. Mouse

5.1.1. Mouse strains

The mouse lines described below were crossed with each other to generate a genetically defined endogenous intestinal carcinoma model. The conditional Cre / loxP system was partly used in the mouse models. Mice that have a transgene inactivated via a loxP-stop-loxP cassette (LSL) can be crossed with a mouse line that has a Cre recombinase driven by a promoter at specific tissue. This leads to a conditional inactivation of the LSL and thus to expression of the target gene at specific tissue. All animal experimentation has been approved by the government of Upper Bavaria, Germany.

Villin-Cre (Braunstein et al., 2002)

Villin-Cre engineered genetic mice have the murine Villin promoter to directly express Cre recombinase at epithelial cells of the SI and LI, in a way that closely minics endogenous Cre recombinase expression. When crossed with a line including a loxP site-flanked site of interest, Cre-induced recombination leds to tissue-specific inactivation of the target. The expression of *Villin-Cre* is generally continuous, however, a small amount of epithelial cells mosaicism is observe d in the colon.

Pik3ca $^{H1047R/+}$ (Eser et al., 2013)

Pik3ca genetic mutation is frequently found in human cancer and *Pik3ca* instructs the produce of p110α of PI3K. H1047R mutation is in the kinase domain of PI3K and an H1047R mutant form of *Pik3ca* was targeted to the Gt (ROSA)26Sor locus behind a floxed PGK-Neo stop cassette. + represents allele from C57BL/6J mice.

Pdk1$^{fl/fl}$ (Lawlor et al., 2002)

In *Pdk1*$^{fl/fl}$ mouse line, loxP sites are flanked before exon 3 and after exon 4. Deletion of exons 3 and 4 through the Cre recombinase eliminate the expression of the *Pdk1* protein.

Pdk1$^{K465E/fl}$ (Bayascas et al., 2008)

In *Pdk1*$^{K465E/fl}$ mouse line, there is a point mutation of lysine 465 in exon 12 of the *Pdk1* gene to glutamic acid. This mutation leads to a change in conformity in the PH domain of the *Pdk1* gene and thereby causes an inhibition of the binding of PDK1 to PIP3. However, PDK1 is expressed normally.

Cre-ER^{T2} (Schonhuber et al., 2014)

This knock-in *Cre-ER*^{T2} mouse line was created in Prof. Saur´s lab. The *Cre-ER*^{T2} mice will produce the tamoxifen-inducible fusion Cre protein by charge of the promoter alleles. The *Cre-ER*^{T2} mice can be used to generate conditional mutations for exploring gain or loss of genetic function.

5.1.2. Genotyping

Around the age of 2 to 3 weeks of pups, an ear biopsy was taken with a special hole puncher when the pups were anesthetized. Silver nitrate applicators were used to disinfect the ear wound. Each mouse was labelled by explicit earmarks which represent a specific number code. The the DNA of biopsy was extracted as described in 5.4.1.

5.1.3. Mouse dissection

Before dissection, the animals were anesthetized with isoflurane then were euthanized, then fixed and disinfected the skin with 75% ethanol. Measure the body weight and cut the abdominal skin and fascia and take all samples by sterile instrument. Measure the length of intestinal tissue and wash with PBS. Intestinal scraping samples were taken using a cover grass to harvest epithelium layer not muscle layer. SilentCrusher M is

applied to crush intestinal scraping samples for RNA and protein isolation. For RNA, intestinal samples in 600 µL RLT buffer and for DNA, 600 µL IP buffer were used. All mouse samples were freshly snap-frozen and then stored at -80°C. The intestines, kidneys, lungs, heart, pancreas, liver, spleen and stomach were fixed in 4% Histofix more than 24h for further histological assays.

5.2. Histology

5.2.1. Paraffin sections

The samples were fixed for histological assays with 4% Roti® Histofix for 24 hours and were dehydrated by the tissue processor ASP300, then embed in paraffin, and kept at room temperature. For subsequent staining, sections (thickness around 1.5µm) were taken via a microtome Microm HM355S.

5.2.2. Hematoxylin and eosin (H&E) staining

The embedded sections were removed wax by incubation (2 x 5 minutes) in Roti® Histol, rehydrated with a series of ethanol solutions (99% twice, 96% twice and 80% twice) and cleaned twice with water. The section was then placed in hematoxylin for 10 seconds, and then blued by immersing the glass slide in tap water for about 5 minutes. Then the slides were incubated in eosin around 15 seconds, then cleaned again in water, and incubated to a series of ethanol solutions (80% twice, 96% twice and 99% twice) and put in Roti® Histol (2 x 5 minutes) then seal with mounting media and a cover slip.

5.2.3. Alcian blue staining

Dewax and rehydrate the paraffin-embedded slides were mentioned in 5.2.2. Alcian blue staining was then carried out by putting the slide in Alcian blue solution for 5 minutes. After cleaning it with water, the samples were counter-stained with nuclear fast red regents for 5 minutes, rehydrated by an ascending ethanol series and mounted according to the instructions in 5.2.2.

5.2.4. Immunohistochemistry

Dewax and hydrate the paraffin-embedded tissue slides were described in 5.2.2. Antigen retrieval was done via cooking the slides in a citrate-based antigen unmasking solution in microwave at 360 W for 10 mins. After cooling down in citrate solution for at least 20 minutes, the slides were rinsed with water once and incubated in 3% H_2O_2 (hydrogen peroxide) for 15 minutes without light to inhibit activity of endogenous peroxidase. Next,sections were rinsed and washed with PBS 3 times, and then blocked with 5% serum in PBS for 1 hour at RT.

The slides were rinsed again with PBS three times and incubated with the primary antibody (ranges from 1:50 to 1:1000) diluted in PBS with 5 % serum at 4 °C more than 24h. Then use the avidin/biotin kit. The day after, slides were washed with PBS three times before applying the secondary biotinylated antibody (1:500), which was diluted in PBS with 5 % serum, for 1 hour at RT. Sections were rinsed again with PBS. The ABC kit Vectastain® elite and the DAB kit were applied under the instructions of manufacturer. The sections were stained again with hematoxylin and then were mounted as mentioned in 5.2.2.

5.2.5. Analysis of staining

In order to record the results of H&E staining, IHC staining, count Ki67-positive cells, an Aperio Versa 8 Digital Scanner was used to photograph the slides. In the results section, representative images are shown. The scale bar usually indicates 100 μm. Quantification by Image J and grading of mice were based on 3 mice at six months and minimal three slides per mouse (Boivin et al., 2003).

5.3. Organoids culture

The organoid cultures established for this study were obtained from genetically engineered mouse models (GEMMs) generated at the Saur lab.

5.3.1. Preparation of L-WRN medium

For maintaining the highly proliferative state of the epithelial stem cells in the organoids cultures, L-WRN conditioned medium was used. L-WRN was prepared using L-WRN cells that secrete Wnt3a, Rspondin and Noggin in the conditioned medium (Koo et al., 2011; T. Sato et al., 2011). L-WRN cells were thawed and seeded on T75 cm flasks and were supplemented with 20 ml medium containing DMEM, 10% FCS, 1% PenStrep and 1% L-glutamine. When the L-WRN cells reached confluency, they were passaged first to four T175 cm flasks and eventually to 16 T175 cm flasks and supplemented with culture medium. On achieving > 90% confluency, the medium was discarded from all the 16 flasks, and the cells were supplemented with 20 ml harvesting medium containing advanced DMEM/F12, 10% FCS, 1% PenStrep, 1% L-glutamine and 1% HEPES. After approximately 24 h, the harvesting medium was collected in 50-ml falcons, and the cells were supplemented with fresh 20 ml harvesting medium. The collected L-WRN was spined down at 2000 × *g* for 5 min to get rid of dead cells as well as debris, and the supernatant was then harvested to 50ml falcons and stored at 4°C until for further use. This procedure of collecting harvesting medium was repeated at the same time interval for 5 days. The collected L-WRN was then filtered through 100 µm filters for avoiding to transfer dead cells to the L-WRN. Subsequently, 20 ml was distributed to new 50-ml flasks and topped up with 20 ml advanced DMEM/F12. Finally, the freshly prepared L-WRN was stored at -80°C. Before use, L-WRN was thawed in the water bath at 37°C.

5.3.2. Isolation of organoids from small and large Intestine

Duodenum and colon tissue samples were taken from the gut of the mouse after flushing the lumen of the gut with ice-cold PBS. The tissue samples were then longitudinally cut for washing with ice-cold PBS to remove mucus or faecal remnants. After washing, the samples were dissected into small fragmentss (<5 mm) and transferred to 50ml falcon with around 20 ml ice-cold 5 mM EDTA for duodenum while

30 mM EDTA for colon. The samples were then incubated for 10 min on ice with intermittent gentle shaking. The supernatant was discarded containing the villi, filtering the solution via a 100µm cell strainer, and was replaced with 20 ml 5 mM or 30 mM EDTA. This process of incubating the tissues with 5 mM or 30 mM EDTA, discarding of supernatant and filtering was repeated three times. After replacing 20 ml ice-cold 5 mM or 30 mM EDTA for the third time, the falcons were vigorously shaken for 30 s, followed by 5 min of incubation and shaking further for 30 s. For colon organoids, this process was repeated at least 3–4 times until a sufficient number of crypts was reached (determined by the turbidity of the supernatant). The solution was then filtered via a 100 µm strainer and then via a 70 µm strainer. This solution was further moved to a 15-ml falcon and spinned down for 5 min at 350 × *g*. Then, the supernatant was discarded, and the leftover pellet was resuspended in 1 ml PBS and spinned down for 5 min at 350 × *g* at 4°C. Discard the supernatant and the pellet was then resuspended in matrigel (50 µl per well), depending on the amount of the pellet. Generally, a maximum of four wells were plated for freshly isolated organoids. The matrigel with cells was plated on pre-warmed (10–20 min at 37°C) 24-well plates in a bubble and incubated at 37°C for allowing the matrigel to polymerize. After the polymerization of matrigel for 10–15 min, L-WRN medium (500 µl per well) with rock inhibitor (5 µl per 500 µl) was added and the plate was stored in the incubator at 37°C.

5.3.3. Isolation of organoids from tumors

Tumour tissue was resected from the mouse and placed in ice-cold PBS. The tumour tissue was then transferred to a petri dish for removing necrotic tissue. The tumour tissue was then transferred to a 15ml falcon and washed with cold PBS three times, followed by mincing into small parts. The minced tumour tissue was then moved to a 1.5ml vial containing 1ml PenStrep for 15 min incubation. After incubation, the tube was spinned down at 350 × *g* for 5 min, rinsed once with PBS and spinned down again for 5 min at 350 × *g*. For digestion, the tumour tissue was incubated at 32°C for 20 min with 1ml PBS containing 10U collagenase type I. The digested tissue was then

transferred to a 15ml falcon and washed with additional 5ml PBS by gentlely pipetting. This suspension was then filtered through 100 µm cell strainer and spinned down at for 5 min 350 × *g*. Discard the supernatant and replaced with 1ml 10% FCS in PBS for 10 min to neutralize the collagenase activity, then centrifugated at 350 × *g* for 5 min. Subsequently, organoids pellet were washed with 0.5 ml cold PBS and sipnned down for 5 min at 350 × *g*. Finally, the organoids were resuspended in matrigel and plated as mentioned in 5.3.2.

5.3.4. Organoid cultures

Organoid cultures were kept at 37°C and 5% CO_2 for 4–9 days, depending on their growth, until further passage or processing. For organoid passage, 300 µl of cell recovery solution was added and was incubated at 4°C for 25–30 min. The matrigel with organoids was then resuspended in the cell recovery solution by vigorous pipetting for dissociating the organoids. The solution was then transferred into 1.5ml virals and spinned down at 350 × *g* for 5 min. Remove the supernatant, and new matrigel (50 µl per well) was added to the organoids pellet and the amount of matrigel rely on the number of wells to be plated required for future use. The matrigel was plated on the 24-well plate and kept at 37°C for 10 min until it had polymerized. After polymerization, L-WRN medium (500 µl) with rock inhibitor (5 µl) was added to each well. The passaged organoid lines were then stored in the incubator at 37°C. For maintenance between passages, yellowish L-WRN medium was replaced with new L-WRN medium without rock inhibitor.

5.3.5. Isolation of DNA

Organoid cell pellets were collected from 3–4 wells per organoid line by instant freezing in liquid nitrogen for DNA isolation. The pellets were then stored at -80°C. After collecting cell pellets from all the organoid lines, DNA was extracted under the introductions of QIAamp® DNA Mini Kit. As a control, a small piece of tail was collected from mice of the respective organoid lines. All the steps for DNA isolation were carried

out under the instructions of manufacturer. The pellets were thawed on ice before DNA isolation. Then, Buffer ATL (180 µl) and proteinase K (20 µl) were mixed to the tubes with samples. The tubes were then vortexed and shaked at 56°C on a thermomixer (1 hour for organoid pellets and overnight for tail samples). After lysis, Buffer AL (200 µl) was added and mixed for 15 s. The tubes were then incubated at 70°C for 10 min. Subsequently, add ethanol (200 µl) to the tubes and mix for 15 s. The solution was pipetted onto the QIAamp Mini spin column upon a 2 ml collection tube and spinned down at 6000 × *g* (8000 rpm) for 1 min. Then the liquid was discarded, and put the QIAamp Mini spin column on a new collection vial. For removing the impurities by washing, the previous washing step was repeated after the addition Buffer AW1 (500 µl). The liquid was discarded, and the QIAamp Mini spin column on a new 2 ml collection vial for second washing step. The tubes were spinned down at full speed (14,000 rpm) following Buffer AW2 (500 µl). The QIAamp Mini spin column were put on a collection vial and then spinned down at 14,000 rpm for 1 min to remove the Buffer AW2. Finally, 35–50 µl of Buffer AE was carefully added to the column and incubated for 1 min before DNA elution in a 1.5 ml tube at 6000 × *g* (8000 rpm) for 1 min. The concentration was measured using Nanophotometer, and the vials were then kept at -80°C until further use.

5.3.6. Isolation of RNA

Organoid pellets were collected from 3–4 wells per organoid line by instant freezing in liquid nitrogen for RNA isolation. The pellets were kept at -80°C. After collecting pellets from all the organoid lines, RNA was harvested using RNeasy® Mini Kit. The pellets were resuspended with 70% ethanol and mixed well. Up to 700 µl of the solution was moved to an RNeasy Mini spin column placed in a 2 ml vial and spinned down for 15 s at ≥8000 × *g*. Discard the flow-through, and DNase digestion was performed. For DNase digestion, Buffer RW1 (350 µl) was put to the spin column and spinned down at ≥8000 × *g*. Discard the flow-through and add DNase I (80 µl) to the column and incubate for 15 min at room temperature. DNase I solution was a mixture of 550 µl RNase-free water and the DNase I.

Then, DNase I solution (10 µl) was put into Buffer RDD (70 µl) and this mixture will be used to incubate the RNeasy column at RT for 15 min. Afterwards, add Buffer RW1 (350 µl) to the RNeasy column and spinned down for 15s at over 8000 × *g* and then remove the flow-through. Add Buffer RW1 (700µl) to the RNeasy spin column and spin down at over 8000 × *g* for 15 s and abandon of flow-through. This washing step was carried out again with 500 µl Buffer RPE. Add Buffer RPE (500µl) to the RNeasy column and spind down at over 8000 × *g* for 2 min. Subsequently, the RNeasy column was put in a 2ml tube for centrifugation at full speed for 1 min. For RNA elution, RNeasy column was put in a 1.5ml tube and add 35 µl RNase-free water to centrifuge column at over 8000 × *g* for 1 min. The elution process was repeated with the same eluate to get a higher amount of RNA. The concentration was checked, and RNA was kept at -80°C.

5.3.7. Mycoplasma contamination test

To detect the contamination of organoid lines with mycoplasma and for quality control check, a PCR for mycoplasma test was performed on all the organoid lines. In place of a DNA template, 2 µl media was taken from one well each of all the organoid lines. Positive band at around 520 bp (base pair).

Table 14. Mycoplasma test PCR

Reaction Mixture		**PCR setup**		
15 µL	REDTaq® ReadyMix™	95 °C	15 min	
2 µL	Reverse-Primer-Mix	94 °C	60s	40x
2 µL	Forward-Primer-Mix	60 °C	60s	
9 µL	H2O	74 °C	60s	
2 µL	DNA template	72 °C	10 min	

5.3.8. Microscopy

Tile scans (3 × 3) were performed for all the slides at 40X. The images were processed with Leica Application Suite X software and ImageJ. Slides were scanned as a test sample using Aperio Versa 8 Digital Scanner.

5.3.9. Organoids 4-hydroxytamoxifen treatment

To induce *CreER^{T2}* in organoids, organoids were added with 1 µM ethanol or 1 µM 4-hydroxytamoxifen (TAM) for 3 days to remove *loxP*-silenced sites. Passaging of organoids and the day after passaging start with tamoxifen treatment. Add 1µl tamoxifen (stock. conc. 500µM) to 499µl L-WRN medium. As control treat some organoids of the same line with ethanol (1µl ethanol per 499µl medium). Incubate for 3 days in the incubator. In case the medium needs to be changed, replace it with fresh L-WRN medium containing tamoxifen or ethanol. After 3 days of Tamoxifen treatment, change medium and replace it with L-WRN medium. Harvest the pellets when organoids are really dense and was stored at -80 °C.

5.4. Molecular techniques

5.4.1. Isolation of DNA

For regenotyping and recombination test PCRs, DNA was extract from tail biopsies using a lysis solution of 50 µl vor Soriano buffer, 1 µl proteinase K and 0.25 µl DTT per sample. The samples were incubated in ThermoQ® at 55°C for 1.5 h, followed by 15 min of heat inactivation of proteinase K at 95°C. The tubes were vortexed and spined at 10,000 rpm for 10 mins, and the supernatant with DNA was moved to a new tube and stored at -20°C.

5.4.2. Polymerase chain reaction

PCR mix buffer, dNTPs and polymerase were used for genotyping or PCR (Mullis et al., 1992) (Table 15). The PCR reaction conditions are listed in Table 16. The amounts of primer were optimized based on the PCR products. PCR products were then stored at 4 °C.

Table 15. Composition of PCR mix

Mixture	Volume for one reaction (µL)
dH2O	4.375
10x buffer S	2.5
30% sucrose	2.5
dNTPs (each 10 µM)	0.5
SucRot	2.5
PeqTaq	0.125

Table 16. Reaction mixture and setup for PCR

Reaction Mixture		Setup conditions		
1.5 µL	DNA	95 °C	3 min	
0.25–2 µL	forward primer	95 °C	45 s	40x
0.25–2 µL	reverse primer	55 °C–72 °C	1min	
12.5 µL	PCR pre-mix	72 °C	90s	
Add until 25 µL	dH2O	25 °C	hold	

Recombination PCR and genotyping. To examine the genotype of mice, DNA of tail or ears biopsies was extracted as mentioned in 5.4.1. Primers for alleles were produced specificly (Table 5). Annealing temperature for different products are shown in Table 17.

mut (refer to the mutated site); WT (refer to the wild type site); rec (refer to after recombination, the mutated site without the stop element)

Table 17. Annealing temperature and products

Name	Annealing temperature	Products (bp)
Villin-Cre	62 °C	1100bp(mut)/200 bp (WT)
CreER^{T2}	55 °C	190 bp (mut)/330 bp (control)
Pdk1^{lox}	63 °C	280bp (mut) / 200bp (WT)
Pdk1^{K465E}	63 °C	236 bp(mut) /196 bp (WT)
Pdk1^{lox} recombination	63 °C	250bp (rec) / 380bp (mut) / 350bp (WT)

Pik3ca^{H1047R} stop	64 °C	630bp (mut)
Tva	62 °C	310bp (mut Tva), 410bp (mut pAe5) 600 bp (WT)

5.4.3. DNA separation

The nucleic acid was splited by electrophoresis in a 1% agarose gel. Dissolve the agarose in TAE buffer by cooking in the microwave. Add ethidium bromide intercalated into the nucleic acid to the gel before gelation. The DNA sample was pipetted into a gel pocket and splited at 120V. For recording, the nucleic acid was photographed by excitation with ultraviolet light.

5.4.4. RNA isolation

RNA isolation from cells. To extract RNA, 600 µL of RLT buffer was added to the tissue/cells, supplemented with 6 µL of 2-mercaptoethanol, and the lysate was collected and stored at -80°C. QIAshredder column and RNeasy mini kit were used for RNA isolation. Use RNase-free DNase group to digest DNA. Use the NanoDrop 1000 spectrophotometer to measure the RNA concentration, and store the sample at -80°C.

cDNA synthesis Follow the manufacturer's instructions and use TaqMan® reverse transcription reagents for cDNA synthesis. Usually, 2 µg RNA was used to generate cDNA and stored at -20°C.

5.4.5. RNA sequence

To examine different gene signatures and potential pathways, genome-wide expression analysis was performed on mouse intestinal tissues and organoids. Extraction of mRNA as mentioned in 5.4.4. The quality was examined by splitting up approximately 500 ng RNA under 80 V on an agarose gel (1%). Good quality samples have a strong 28S and a 18S ribosomal RNA (rRNA) band, respectively. The intensity of the 28S rRNA band is usually about 1.5 times to 2.5 times that of the 18S rRNA band. Take 2 µg of RNA and use the TruSeq® chain mRNA preparation kit to use

Agencourt AMPure XP Beads and SuperScript II as reverse transcriptases for Illumina sequencing. After the first and second strands of cDNA are synthesized, adaptor ligation is performed, and nuclear acid pieces with adaptors at both sides are amplified by PCR. The integrity of the cDNA needs to be tested by qRT-PCR using the barcode-specific primers added, and use the Qubit®dsDNA BR Assay Kit on Qubit to determine the quantity® 2.0 Fluorometer. Combine high-quality samples with sizes of 200-500 bp then submit 50 bp single-read sequence on the Illumina HiSeq2500 platform of the TranslaTUM facility. TopHat was used to align the reads with the mouse genome (Trapnell, Pachter, & Salzberg, 2009).

Bcl files produced by Illumina Nextseq sequencer were then converted to fastq using bcl2fastqtool (version: v2.17.1.14), setting parameters as default values. Quality control was performed by FastQC (version: v0.11.5, Babraham Institute). Converting fastq files to bam files was done by using FastqToSam command of Picard tools (version: 1.138, Broad Institute). Cell barcode and molecular barcode were extracted by Drop-seq tools (McCarroll Lab, http://mccarrolllab.com/dropseq/) version 1.12 Tag Bam with Read Sequence Extended programme. Low quality reads were filtered out using Drop-seq tools version 1.12 Filter BAM program. Drop-seq tools version 1.12 PolyATrimmer script removed poly-A/T outputting bam files that were then converted to fastq files by SamToFastq of Picard tools (version: 1.138). Star (version: 2.5.3) aligned the resulting reads to mouse genome (mm10). Output bam files were sorted using Sort Bam. Then Merge Bam Alignment merged aligned and unaligned bam files. These two commands were provided by Picard tools (version 1.138). Drop-seq tools version 1.12 Tag Read with Gene Exon assigned gene symbols to each record, where gene symbols were from its integrated annotation files. Drop-seq tools version 1.12 Digital expression then generated read count matrix using the resulting bam files.

Differential gene expression analysis was done using edgeR and limma R packages. Raw read counts were log2-counts per million (log-cpm) transformed. Genes with log-cpm less than 1 in more than 25% samples were filtered out. Calculating sample-wise

normalization factor based on trimmed mean of M-values (TMM) method on the remaining genes and transforming counts to log-cpm by voom function, we fitted a linear model with genotype as input and gene expression level for each gene as response variable: y_g = m. Where y_g is the gene expression vector of gene $_g$ across samples, m is a sample*genotype coefficient matrix of that element set to 1 if one sample has a specific genotype otherwise set to 0. With this model we selected top differential genes to produce heatmap according to FDR-adjusted p values (threshold: p <= 0.05). Gene set enrichment analysis (GSEA) was operated with GSEA java package provided by Broad institute, using curated gene sets (C2) of the Molecular Signature Database (MSigDB).

5.4.6. Low coverage whole genome sequencing

Genome DNA was extracted as the method mentioned in 5.3.5. Low coverage whole genome sequencing was processed by using Hiseq 2000 after quality control. Raw data were cleaned by FastQC to remove low-quality reads. Burrows-Wheeler Aligner was used to blast short sequences to reference sequences. To remove duplication and detect mutations, Genome Analysis Toolkit (GATK, http://www.broadinstitute.org/gatk/) and SegSeq were used to carry out CNV analysis. Afterward, R studio was used to analyze segment files.

5.4.7. Whole exome sequencing

Genome DNA was extracted as the method mentioned in 5.3.5. Whole exome sequencing was processed by using Hiseq X after quality control. Raw data were cleaned by FastQC and multiQC and trimgalore to remove not useful sequencing. Burrows-Wheeler Aligner was used to blast short reads to reference sequence. Bamqc in qualimap was used to blast bam files. Genome Analysis Toolkit (GATK, http://www.broadinstitute.org/gatk/) was used to get on target bases, on target and near target bases, mean target coverage, and target region coverage, and detect

mutations. Annovar was used to get annotations. Afterward, R studio was used to analyze maf files by maftools packages.

5.5. Statistical analysis

GraphPad Prism 8 was applied for drawing graph and statistical analysis. Unless otherwise indicated, all raw data are processed from 3 independent experimental groups at least and were showed as standard error of the mean (SEM) or mean ± standard deviation (SD). Kaplan-Meier analysis and log-rank test were applied for survival analysis. Statistical analysis for RNA sequence was described in 5.4.5 and R studio (Version 1.3.959) was used.

6. Results

6.1. *Pik3ca* activation has different effects on the small intestine and the large intestine

To elucidate the role of *Pik3ca*^{H1047R} in the intestine, the Saur lab previously generated transgenic mice with conditional activation of *Pik3ca*^{H1047R} (encoding p110α^{H1047R}) in intestinal epithelial cells (IECs) mediated by Cre recombinase that is driven by the IEC-specific promoter Villin (*Villin-Cre*), resulting in the dominant expression of the H1047R mutant PI3K protein. Upon activation of Cre, a lox-stop-lox cassette at the *Pik3ca* site of the mouse Rosa26 locus is removed, specifically from the small intestine, large intestine, and cecum but not in other organs. Without the existence of Cre, the lox-stop-lox cassette prevents the production of mutant PI3K. In the following paragraph these data that are part of the doctoral thesis of Regina Pietsch are partially described and shown in Fig. 1 to demonstrate the phenotype of this unpublished work. The detailed work and characterization of the mouse line will be presented in the doctoral thesis of Reginal Pietsch.

Survival analysis of all *Pik3ca*$^{H1047R/+}$ and *Pik3ca*$^{H1047R/H1047R}$ animals in her cohort revealed that small intestinal tumors developed in these groups and the mice showed a significant decrease in survival versus control mice (Figure 1C). Homozygous *Pik3ca*$^{H1047R/H1047R}$ exhibited medial survival times approximately 145 days shorter than the heterozygous *Pik3ca*$^{H1047R/+}$ cohort, which was slightly different than the wild-type. The majority of oncogenic *Pik3ca* mice (include homozygous and heterozygous *Pik3ca* mice, the following as same) became moribund in the range of 400 and 700 days of age. Metastatic lesions in lymph nodes, liver, lung, and kidney due to small intestine tumors were found in 18% of *Pik3ca*$^{H1047R/+}$ mice and 26% of *Pik3ca*$^{H1047R/H1047R}$ mice. (Figure 1B). The phenotypes of the small intestinal tumors were similar in homozygous and heterozygous *Pik3ca* mice since adenoma, cystic adenoma, adenocarcinoma,

carcinoma and mucinous carcinoma were found in both two groups. In *Pik3ca*$^{H1047R/+}$ mice group, the ratio of adenoma and adenocarcinoma was increased and the ratio of cystic adenoma, carcinoma and mucinous carcinoma was decreased compared to that of *Pik3ca*$^{H1047R/H1047R}$ mice group.

The entire homozygous and heterozygous *Pik3ca*^{H1047R} mice cohort showed the earliest tumor initiation, dated to approximately 6 months, and the average number of tumors, including adenomas and carcinomas, was one or two per mouse. Tumor formation in *Pik3ca*$^{H1047R/+}$ and *Pik3ca*$^{H1047R/H1047R}$ mice was strikingly similar, with close similarities in the number of tumors for each mouse and time distribution of tumor formation (Figure 1D).

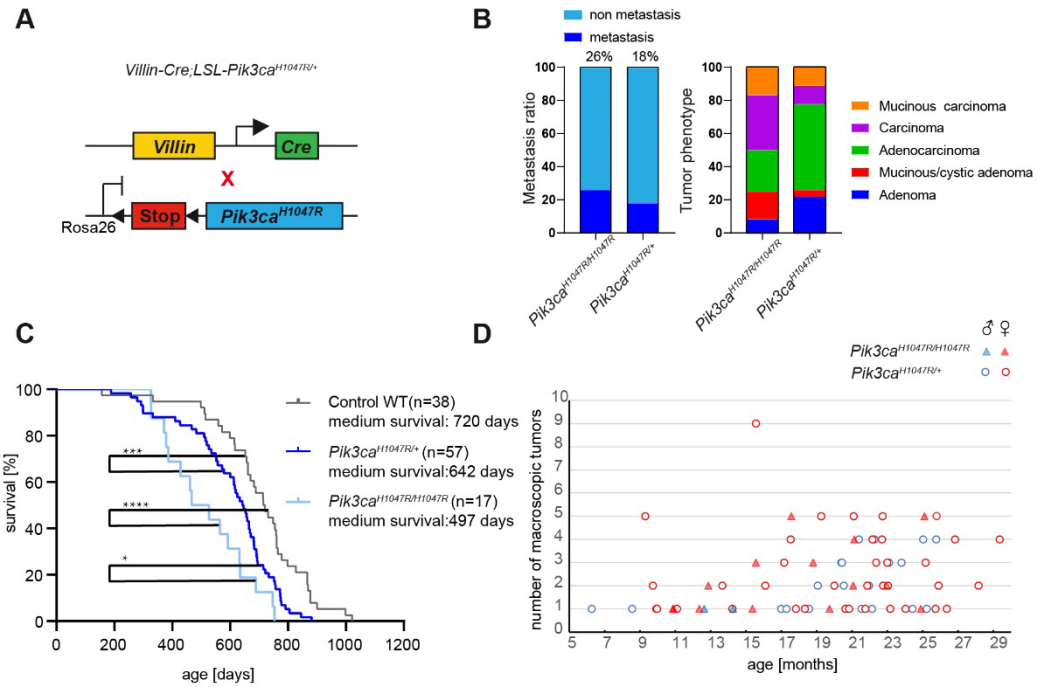

Figure 1. Oncogenic *Pik3ca* initiates small intestine tumorigenesis

(A) Genetic strategy used to activate *Pik3ca*^{H1047R} expression in the intestine.

(B) Kaplan-Meier survival analysis of wild-type mice, *Pik3ca*$^{H1047R/+}$ and *Pik3ca*$^{H1047R/H1047R}$ mice. + stands for the wild-type allele (*p < 0.1; ***p < 0.001; ****p < 0.0001, log-rank test).

(C) The ratio of tumor mice with metastasis in *Pik3ca*$^{H1047R/+}$ (n=57) tumor mice cohort and *Pik3ca*$^{H1047R/H1047R}$ (n=17) mutant mice at left side. The distribution of tumor phenotypes in indicated mice cohort were showed at right side.

(D) Overview of intestinal tumors development in *Pik3ca*$^{H1047R/+}$ and *Pik3ca*$^{H1047R/H1047R}$ mice.

Each circle stands for a *Pik3ca*$^{H1047R/+}$ mouse and each triangle stands for a *Pik3ca*$^{H1047R/H1047R}$ mouse (tumors were defined as dysplasia over 2 mm). The number of tumors is showed on the y axis.
(*Pik3ca*$^{H1047R/+}$ mouse line was generated in Saur's lab and these data are part of the unpublished doctoral thesis of Regina Pietsch. Figure 1 is to demonstrate *Pik3ca*$^{H1047R/+}$ phenotype and the detailed work and characterization of the mouse line will be presented in the doctoral thesis of Reginal Pietsch.)

6.2. Blocking *Pdk1* in oncogenic *Pik3ca* intestinal mouse model initiates a mucinous phenotype of CRC at large intestine

PI3K activates multiple downstream signals by transforming PIP2 into PIP3, then PIP3 traffics PI3K signals by connecting proteins such as AKT and PDK1 and then binding them to the cell membrane with PH domains. Previously, our group established a PDK1 inactivation in mice which could completely block PDAC formation in the Kras^{G12D} model and demonstrated *Pdk1* acts as an oncogene. In our oncogenic *Pik3ca* mouse model, the level of PDK1 was increased in the intestine. To address whether the PI3K downstream effector PDK1 is also important for *Pik3ca*-driven CRC, we blocked *Pdk1* in the epithelial cells of the intestine via floxed flanked *Pdk1* mice (Figure 2A). *Villin-cre* induced inactivation of *Pdk1* in the intestine was examined by PCR (Figure 2B). Unexpectedly, the deletion of *Pdk1* in oncogenic *Pik3ca* mice did not result in the development of small intestine tumors but did induce tumors at the large intestine, which is entirely different from the anatomical location of tumors in oncogenic *Pik3ca* mice (Figure 2D). Specifically, in all mice in the *Pik3ca*$^{H1047R/+}$, *Pdk1*$^{fl/fl}$ cohort and *Pik3ca*$^{H1047R/H1047R}$, *Pdk1*$^{fl/fl}$ cohort large intestine tumors were initiated with a steeply decreased median survival of approximately 353 days and 251 days, respectively (Figure 2C). Metastatic lesions in extraintestinal organs were found in 22% of *Pik3ca*$^{H1047R/H1047R}$, *Pdk1*$^{fl/fl}$ mice and 11% of *Pik3ca*$^{H1047R/+}$, *Pdk1*$^{fl/fl}$ mice (Figure 2F). The phenotypes of the large intestinal tumors were similar in homozygous and heterozygous *Pik3ca*, *Pdk1* deletion mice since cystic adenoma, adenoma, mucinous carcinoma were found in both two groups (Figure 2E). In *Pik3ca*$^{H1047R/+}$, *Pdk1*$^{fl/fl}$ mice group, the ratio of cystic adenoma was increased and the ratio of cystic mucinous

carcinoma was decreased compared to that of *Pik3ca*$^{H1047R/H1047R}$, *Pdk1*$^{fl/fl}$ mice group (Figure 2F).

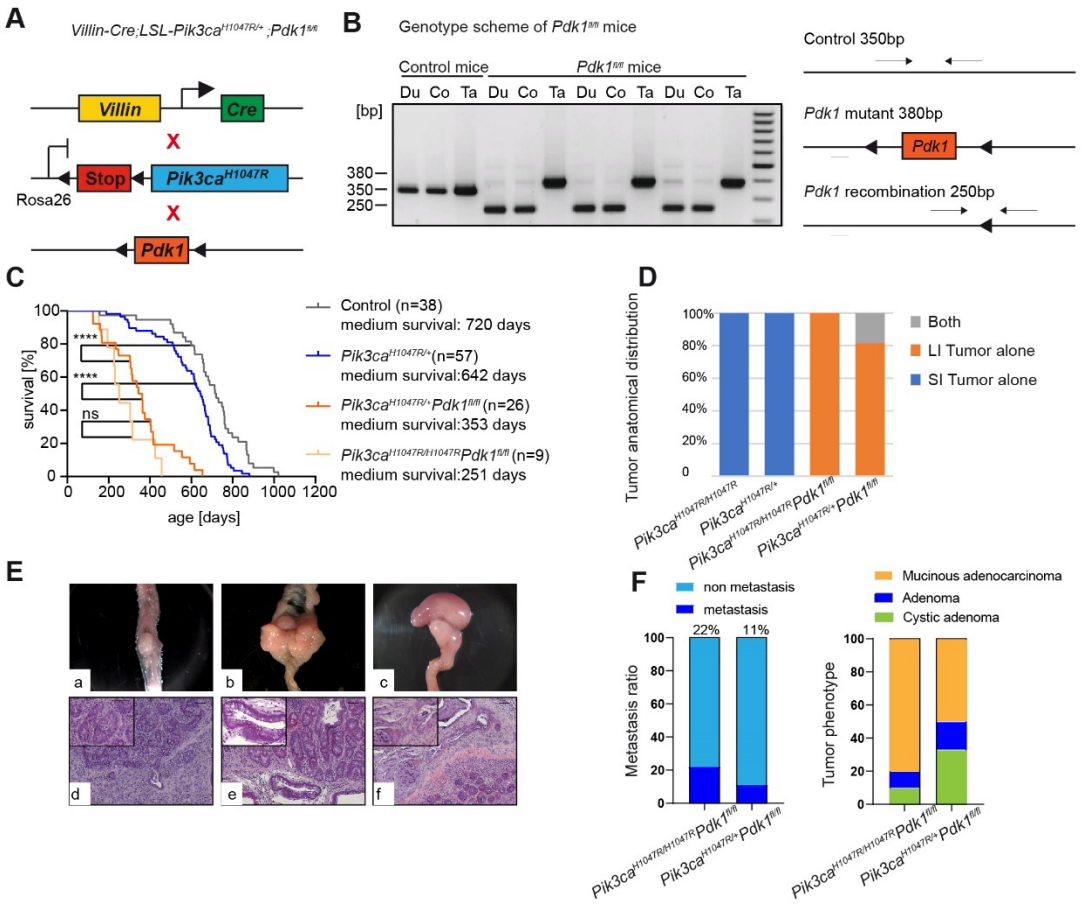

Figure 2. Blocking *Pdk1* in oncogenic *Pik3ca* intestinal mouse model initiates a mucinous phenotype of CRC at large intestine

(A) Genetic strategy to activate *Pik3ca*^{H1047R} oncogenic expression and block *Pdk1* expression in the intestine.

(B) *Villin-Cre*-induced recombination of deleted *Pdk1* in *Pdk1*$^{fl/fl}$ mice. Co, colon; Du, duodenum; Ta, tail.

(C) Kaplan-Meier survival analysis of the indicated mouse lines. + stands for the wild-type allele (ns, not significant; ****p < 0.0001, log-rank test).

(D) Tumor anatomical distribution of the indicated conditional genotypes. *Pik3ca*$^{H1047R/H1047R}$, n=17; *Pik3ca*$^{H1047R/+}$, n= 57; *Pik3ca*$^{H1047R/H1047R}$, *Pdk1*$^{fl/fl}$ n=9; *Pik3ca*$^{H1047R/+}$, *Pdk1*$^{fl/fl}$, n=26;

(E) Representative macroscopic (Ea/ Eb / Ec), microscopic images (Ed/ Ee / Ef), of small intestine tumors from *Pik3ca*$^{H1047R/+}$, *Pdk1*$^{fl/fl}$ mice cohort and *Pik3ca*$^{H1047R/H1047R}$, *Pdk1*$^{fl/fl}$ mice. Scale bars, 100 µm.

(F) The ratio of tumor mice with metastasis in *Pik3ca*$^{H1047R/H1047R}$, *Pdk1*$^{fl/fl}$ (n=9) tumor mice cohort and *Pik3ca*$^{H1047R/H1047R}$, *Pdk1*$^{fl/fl}$ (n=26) mice. The distribution of tumor phenotypes in indicated mice cohort were showed at right.

(Work on the *Pik3ca*$^{H1047R/+}$ -only model has been established by Regina Pietsch and will be presented in detail in her thesis.)

At necropsy, almost all *Pik3ca*$^{H1047R/+}$, *Pdk1*$^{fl/fl}$ and *Pik3ca*$^{H1047R/H1047R}$, *Pdk1*$^{fl/fl}$ mice had neoplastic lesions at the proximal colon (Figure 2E). Based on gross macroscopic observations, mostly large intestinal tumors primarily occurred in the intestinal lumen and were solid and nodular-like with rare hemorrhage. The normal structure of longitudinal mucosal rugal folds disappeared at tissue adjacent to the tumor and was replaced by disorder-thickened stiff rugal folds and mucosa.

To examine the oncogenic PI3K induced different tumor phenotypes, whole exome sequencing was carried out by using cystic tumors (n=2) and solid tumors (n=3) from *Pik3ca*^{H1047R} mice (Figures 3A,3B). From the summary analysis of samples we have now, missense mutation, nonsense mutation and frame shift deletion were the top 3 variants classification in both cystic tumors and solid tumors. The variants type and SNV class did not show differences between cystic tumors and solid tumors. Interestingly, the top 10 mutated genes in cystic tumors group and solid tumors group were quite distinct. Among solid tumors, *Usp9x* and *Olfr748* are both involved in GPCR (G protein-coupled receptor) pathway, *G6pdx* related to pentose phosphate pathway, *Chmp4c* related to necroptosis, *Foxc2* related to glucose and energy metabolism, Huwe1 related to *C-myc* activation, *Kndc1* related to RAS and MAP2, and *Odf2* related to PLK1 (polo-like kinase 1) activity and cell cycle (Figure 3Af). Among cystic tumors, *Apol10b* is involved in binding and uptake of scavenger receptors, *Adamts13* related to O-glycosylation and TSR (thrombospondin type 1 repeat) domain, *Aldh18a1* related to urea cycle and metabolism of amino group, *C4b* related to immune response, *Chd5* related to chromatin regulation and acetylation and *Col5a2* related to intergrin pathway

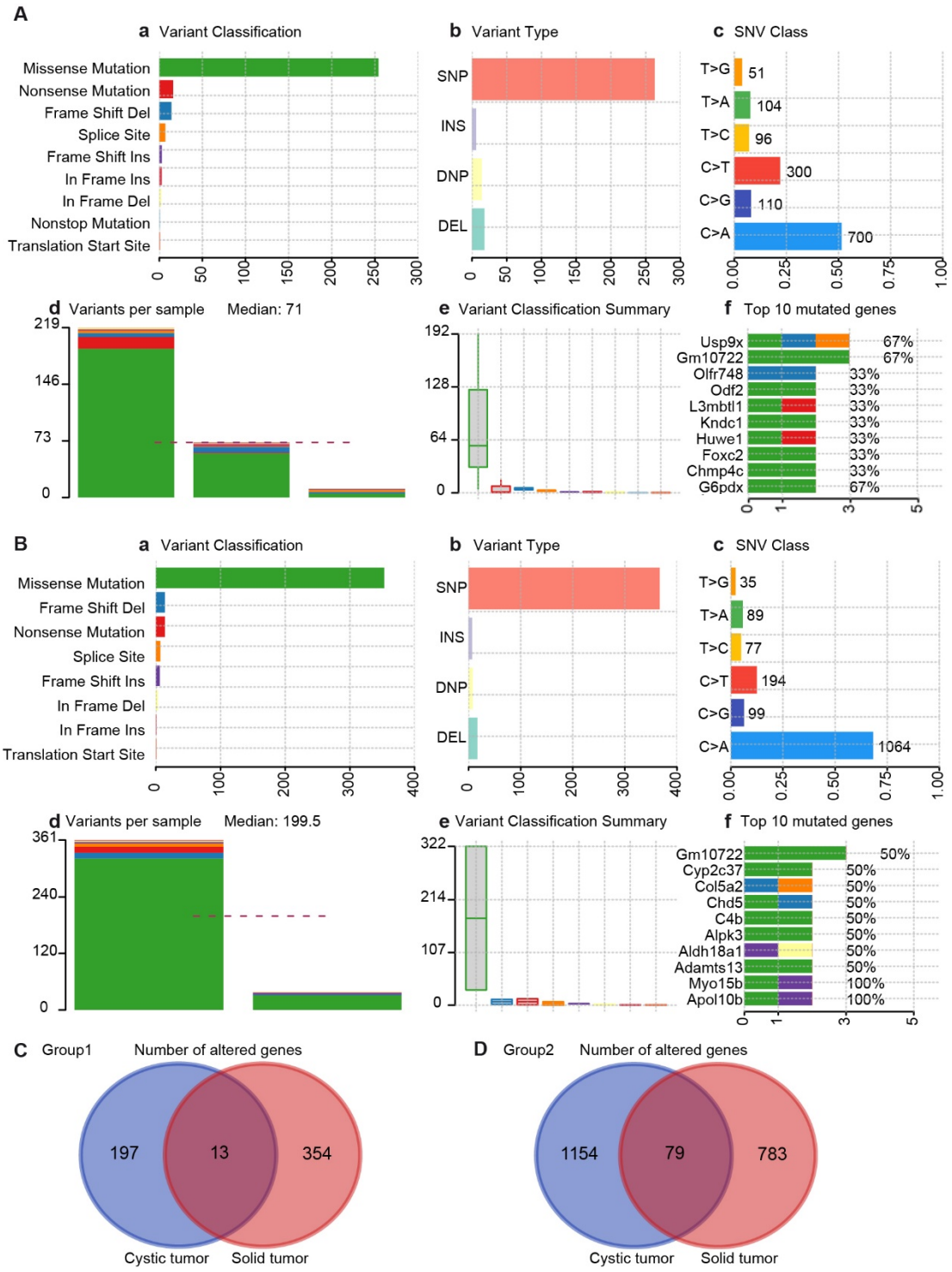

Figure 3. Whole exome sequencing analysis of cystic and solid tumors in *Pik3ca*^{H1047R} mice

(A) Summary of variants type of solid tumors (n=3) from *Pik3ca*^{H1047R} mice. a) number of variants in each sample as a stacked bar plot. (Del, deletion; Ins, insert)b) variant types as a boxplot summarized by variant classification. c) the ratio of different SNV class. d) the number of variants and median of variants for each sample as a histogram. e) summary of variant classification as a boxplot. f) top 10 mutated genes in all samples.

(B) Summary of variants type of cystic tumors (n=2) from *Pik3ca*^{H1047R} mice. a) number of variants in each sample as a stacked bar plot. (Del, deletion; Ins, insert)b) variant types as a boxplot summarized by variant classification. c) the ratio of different SNV class. d) the number of variants and median of variants for each sample as a histogram. e) summary of variant classification as a boxplot. f) top 10 mutated genes in all samples.
(C) Group1, 13 genes were both mutated in cystic and solid tumor from one *Pik3ca*^{H1047R} mouse.
(D) Group2, 79 genes were both mutated in cystic and solid tumor from one *Pik3ca*^{H1047R} mouse.

Table 18. Shared mutations between cystic and solid tumor in same mouse (n=2)

GA: gene name; Chr: chromosome; SP: mutation start position; VC: variant classification; VP: variant type; A1: tumor sequence aelle 1; A2: tumor sequence aelle 2; SNP: single nucleotide polymorphism; DNP: double nucleotide polymorphism; RC: read coverage; AF: allele frequency; (*Gm28992* was not showed in Group1, *Gm44018* was not showed in Group2.)

GA	Chr	SP	VC	VP	A1	A2	CT		ST	
							RC	AF	RC	AF
Group1 (mouse ID: 11596)										
Etnk2	1	133364046	Intron	SNP	T	A	10	0.25	21	0.217
Etnk2	1	133364049	Intron	SNP	G	C	10	0.248	21	0.217
Mcm7	5	138166012	Silent	SNP	G	A	66	0.115	95	0.111
Group2 (mouse ID: 13319)										
Olfr1031	2	85992479	Missense Mutation	SNP	T	A	79	0.22	46	0.124
Ppcs	4	119422159	Missense Mutation	DNP	GC	GC	28	0.2	28	0.2
Ppcs	4	119422163	Missense Mutation	SNP	C	C	28	0.2	28	0.199
Muc5b	7	141871226	Intron	SNP	C	A	37	0.279	27	0.205
Kif2b	11	91576364	Silent	SNP	C	T	66	0.115	64	0.104
Vmn2r97	17	18948135	3'UTR	SNP	T	C	18	0.25	18	0.15

Table 19. The purity of tumor samples in WES analysis

NA: not available (insufficient information to estimate)

Tumor sample	Facets		Sclust	
	Purity	Ploidy	Purity	Ploidy
Group1				
11596-cyst	0.1	2.4	0.2	1.9
11596-solid	0.3	2.2	0.2	2.1
Group2				
13319-cyst	0.3	2.1	NA	NA
13319-solid	0.2	2.3	0.2	2
Group3				
13323-solid	NA	2	0.3	1.9

(Figure 3Bf). In order to compare genetic alterations in solid tumor and cystic tumor from the same mouse, across comparison was operated on two groups. From group1, 13 genes were both mutated in cystic and solid tumor from one *Pik3ca*^{H1047R} mouse ,while among them 10 genes were altered in both tumor but not same variation type and 3 genes were altered in both tumor with the same variation type, that are *Gm28992*, *Mcm7* related to the regulation of activated PAK-2p34 and E2F (The E2 factor family) mediated regulation of DNA replication. *Etnk2* related to metabolism and glycerophospholipid biosynthesis (Figure 4C). In comparison group2, 79 genes were both mutated in cystic and solid tumor from one *Pik3ca*^{H1047R} mouse ,while among them 73 genes were altered in both tumor but not the same variation type and 6 genes were altered in both tumor with same variation type, that are *Muc5b*, related to metabolisms of proteins, *Gm44018*, *Ppcs*, related to pantothenate and CoA biosynthesis and metabolism of water-soluble vitamins and cofactors, *Olfr1031*, related to GPCR and Olfactory transduction, *Vmn2r97*, *Kif2b* related to GPCR and mitotic prometaphase (Figure 4D). Due to the low number of samples for each group, it's not sufficient to draw any conclusions but it's clear that 2 cystic tumors and 3 solid tumors being analyzed exhibited distinct genetic alterations and it's highly possible that two tumor phenotypes in our analysis did not evolve from the same origin.

6.3. *Pik3ca* activation has different effects on the small intestine and the large intestine

To further understand the mechanisms behind tumorigenesis in oncogenic *Pik3ca* mice initiated at the small intestine, not the large intestine, we examined the expression of the transcripts of the intestine. Compared with wild-type control mice, transcripts of 28 genes were found upregulated, and 67 were found downregulated in the small intestine of oncogenic *Pik3ca* mice (Figures 4A-4B). In the large intestine, 40 genes were found upregulated, and 86 were found downregulated (Figures 4C-4D). *Wfdy1* regulating TLR3/4-mediated (Toll-like receptor) signaling pathways, and *Sprr2a3* as a cross-

linked envelope protein of mouse keratinocytes were both upregulated in the small intestine and the large intestine. 3 genes were downregulated including *Ccnd2*,

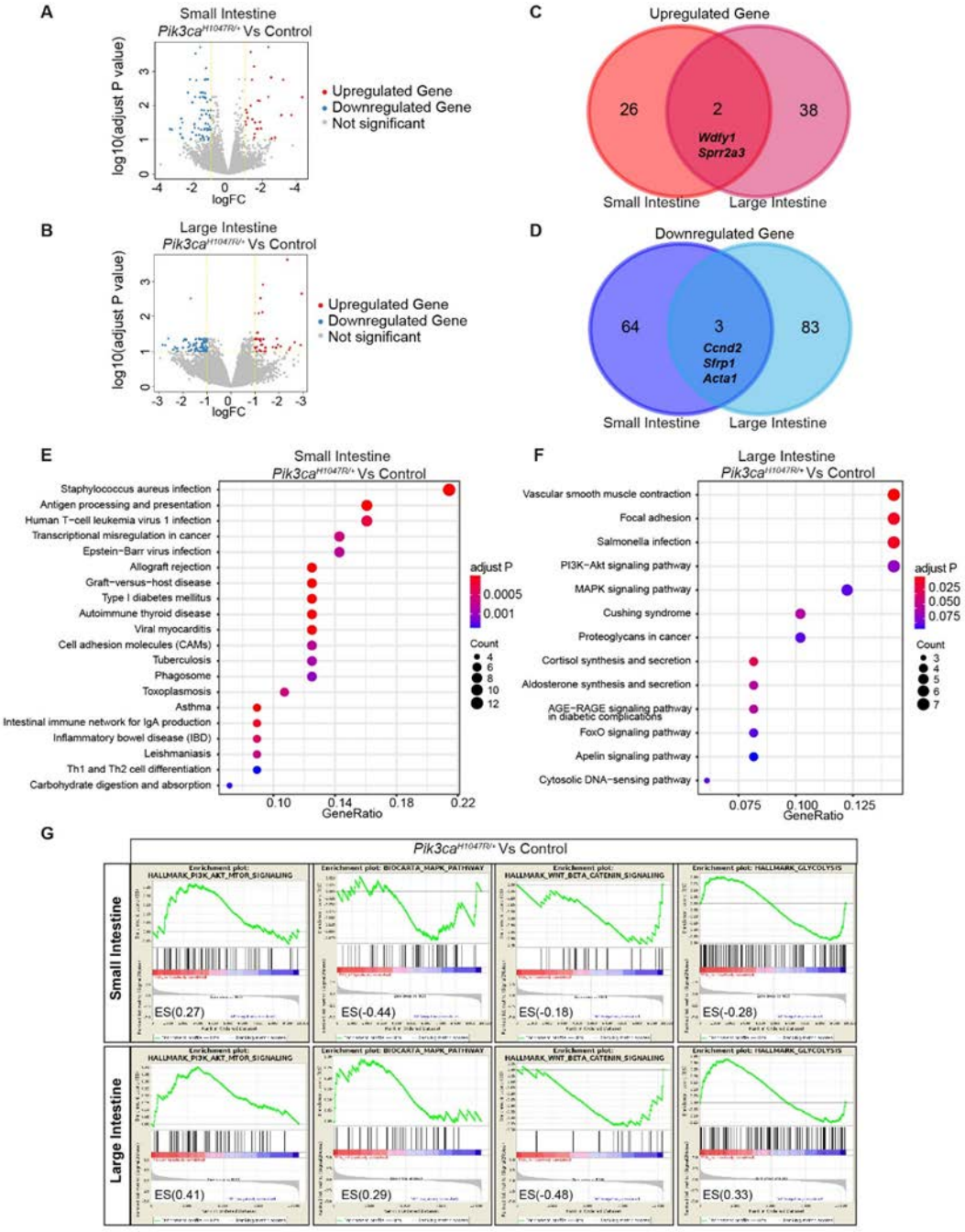

Figure 4. mRNA expression analysis of oncogenic *Pik3ca*^{H1047R} mice

(A) The volcano plot depicting the fold differences in mRNA expression levels of epithelial cells in the small intestine between *Pik3ca*$^{H1047R/+}$ and control mice. Each dot stands for a mRNA, x axis stands for the log value fold change; y axis stands for the log10 of the adjust P value. Significantly up-regulated are showed in red circle and significantly down-regulated in blue.

(B) 2 same mRNAs are shared among up-regulated 26 mRNAs in small intestine and up-regulated 40 mRNAs in large intestine.

(C) The volcano plot depicting the fold differences in mRNA expression levels of epithelial cells in the large intestine between *Pik3ca*$^{H1047R/+}$ and control mice. Each dot stands for a mRNA, x axis stands for the log value fold change; y axis stands for the log10 of the adjust P value. Significantly up-regulated are showed in red circle and significantly down-regulated in blue.
(D) 3 mRNAs are shared among up-regulated 67 mRNAs in small intestine and up-regulated 87 mRNAs in large intestine.
(E) Gene set enrichment analysis of mRNAs sequence of small intestine between *Pik3ca*$^{H1047R/+}$ and control mice by using KEGG.
(F) Gene set enrichment analysis of mRNAs sequence of large intestine between *Pik3ca*$^{H1047R/+}$ and control mice by using KEGG.
(G) Gene set enrichment analysis comparing gene signatures of intestine tissue between *Vil-Cre*, *Pik3ca*$^{H1047R/+}$ and control mice by using hallmark gene sets.
(RNA samples were extracted by Regina Pietsch, RNA sequence was done by Rad Roland's lab and data was analysed by Meng Lei and Xiaoxiao Zhang.)

encoding Cyclin D2 to coordinate mitotic events, *Sfrp1* to encode Sfrp1 protein as a tumor suppressor in many cancer types, and *Acta1* offering instructions for producing a protein called skeletal alpha (α)-actin, which is vital for muscle contraction and cell movement. Though few shared alterations in the SI and the LI of oncogenic *Pik3ca* mice, enrichment analysis showed distinct changes between the SI and the LI (Figures 4E-4F). In the small intestine, oncogenic *Pik3ca*-triggered alterations are mainly related to unusual immune activities and infections, such as antigen processing and presentation, increase IgA production and many immune relevant disease signalings. While oncogenic *Pik3ca*-triggered unusual immune activities were not detected in the large intestine instead of active signalings and chemical synthesis including PI3K/AKT, MAPK, FOXO pathway, and the synthesis of cortisol, aldosterone.

Notably, enrichment analysis demonstrated PI3K/AKT signaling was increased, Wnt signaling and glycolysis was decreased in both the small and large intestine; however, MAPK signaling and was only upregulated in the large intestine. This observation further illustrates that signaling alterations arising by oncogenic *Pik3ca* are distinct in the small intestine and large intestine, and these different signaling activities may play a role in oncogenic *Pik3ca*-induced small intestine tumorigenesis (Figure 4G).

6.4. Distinct RNA sequence patterns between the intestine from *Pik3ca*$^{H1047R/+}$ mice and *Pik3ca*$^{H1047R/+}$, *Pdk1*$^{fl/fl}$ mice

Principle component analysis (PCA) of the small intestine showed *Pik3ca*$^{H1047R/+}$ mice were clustered distinctly differently from *Pik3ca*$^{H1047R/+}$, *Pdk1*$^{fl/fl}$ mice and wild-type control (Figure 5A). KEGG (Kyoto encyclopedia of genes and genomes) enrichment analysis of significant pathways indicated the synthesis of glycosphingolipid, glycan, bile acid, and proteasome were reduced, and selenoamino acid metabolism, as well as the renin–angiotensin system, was suppressed in the small intestine of oncogenic *Pik3ca* mice (Figure 5B). In contrast, the biosynthesis of pyrimidine, arginine, proline, aminoacyl trna, and purine were higher in the small intestine of all oncogenic *Pik3ca* mice and few *Pik3ca*$^{H1047R/+}$, *Pdk1*$^{fl/fl}$ mice. Notably, base excision repair and colorectal cancer-related transcripts were found to increase in both the small intestine of oncogenic *Pik3ca* mice and *Pik3ca*$^{H1047R/+}$, *Pdk1*$^{fl/fl}$ mice.

In the large intestine, principle component analysis indicated *Pik3ca*$^{H1047R/+}$ mice were clustered slightly differently from *Pik3ca*$^{H1047R/+}$, *Pdk1*$^{fl/fl}$ mice and wild-type control (Figure 5C). Base excision repair, DNA replication, and ribosome activity were downregulated in both oncogenic *Pik3ca* mice and *Pik3ca*$^{H1047R/+}$, *Pdk1*$^{fl/fl}$ mice, as well as transcripts related to mTOR signaling and colorectal cancer. The synthesis of pantothenate and CoA, sulfur, glycine, serine and threonine, porphyrin and chlorophyll were upregulated in both oncogenic *Pik3ca* mice and *Pik3ca*$^{H1047R/+}$, *Pdk1*$^{fl/fl}$ mice. However, the IgA immune network was only improved in *Pik3ca*$^{H1047R/+}$ mice (Figure 5D).

Taken together, mostly significant transcript alterations of the intestine in *Pik3ca*$^{H1047R/+}$ mice and *Pik3ca*$^{H1047R/+}$, *Pdk1*$^{fl/fl}$ mice were related to the inorganic formation and amino acid. Furthermore, the comparison of Hallmark and BioCarta enrichment analysis of intestinal transcripts from *Pik3ca*$^{H1047R/+}$, *Pdk1*$^{fl/fl}$ mice and wild-type control mice demonstrated improved PI3K/AKT and Wnt signaling in the small intestine in

Pik3ca$^{H1047R/+}$, *Pdk1*$^{fl/fl}$ mice but both signals were reduced in the large intestine (Figure 5E).

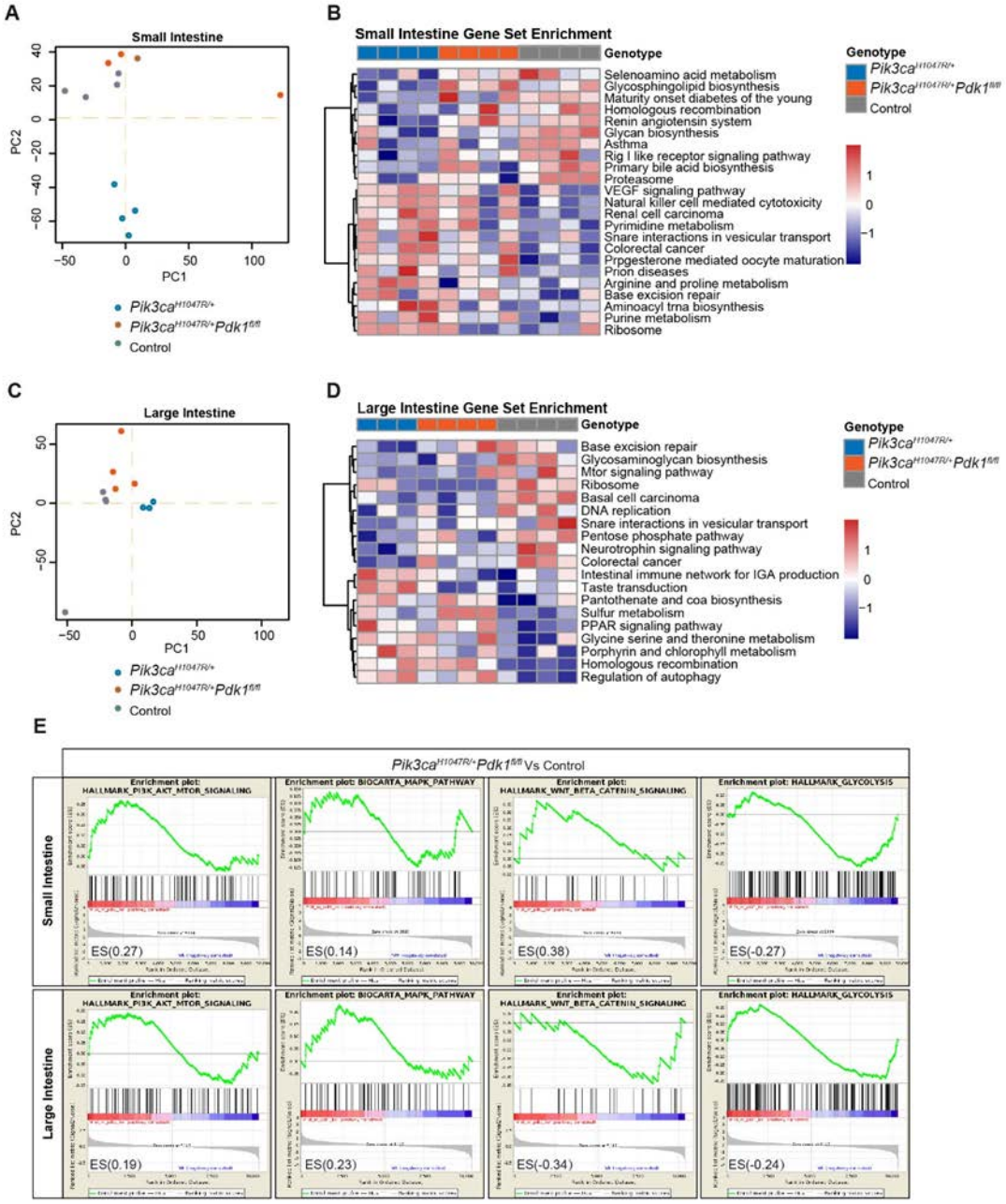

Figure 5. mRNA expression analysis of *Pik3ca*$^{H1047R/+}$, *Pdk1*$^{fl/fl}$ mice

(A) Principal component analysis (PCA) of small intestinal tissue *Pik3ca*$^{H1047R/+}$ mice, *Pik3ca*$^{H1047R/+}$, *Pdk1*$^{fl/fl}$ mice and control mice. Each point corresponds to a sample.

(B) Heatmap of differential mRNA expression of the small intestine in KEGG pathways between *Pik3ca*$^{H1047R/+}$ mice, *Pik3ca*$^{H1047R/+}$, *Pdk1*$^{fl/fl}$ mice and control mice. Pixels stand for Log2 read counts for a pathway. Blue stand for under-expression pathway and red indicate over-expression pathway.

(C) Principal component analysis (PCA) of large intestinal tissue *Pik3ca*$^{H1047R/+}$ mice, *Pik3ca*$^{H1047R/+}$, *Pdk1*$^{fl/fl}$ mice and control mice. Each point corresponds to a sample.
(D) Heatmap of differential mRNA expression of the large intestine in KEGG pathways between *Pik3ca*$^{H1047R/+}$ mice, *Pik3ca*$^{H1047R/+}$, *Pdk1*$^{fl/fl}$ mice and control mice. Pixels stand for Log2 read counts for a pathway. Blue stand for under-expression pathway and red indicate over-expression pathway.
(E) Gene set enrichment analysis comparing mRNA expression signatures of intestine tissue between *Pik3ca*$^{H1047R/+}$, *Pdk1*$^{fl/fl}$ and control mice by using hallmark gene sets.
(RNA samples were extracted by Regina Pietsch, RNA sequence was done by Rad Roland's lab and data was analysed by Meng Lei and Xiaoxiao Zhang.)

6.5. Ablation of *Pdk1* induces large intestine neoplasms

In oncogenic *Pik3ca* with inacitvation of *Pdk1* mice model, the anatomical position of intestinal tumorigenesis shifted from small intestine to large intestine, implying that *Pdk1* may act as a tumor suppressor in the large intestine and an oncogene in the small intestine. To further verify our hypothesis, we only specifically inactivated *Pdk1,* in the epithelial cells of the intestine via floxed flanked *Pdk1* mice to prevent cell-autonomous Pdk1 signaling (Figure 6A). In *Pdk1*$^{fl/fl}$ mice cohort, the median survival was approximately 243 days, which was not significantly different from that of the *Pik3ca*$^{H1047R/+}$, *Pdk1*$^{fl/fl}$ cohort but still markedly decreased from the *Pik3ca*$^{H1047R/+}$ cohort and wild-type control mice (Figure 6B).

All intestinal *Pdk1* deletion mice demonstrated large intestine neoplasms (Figure 6C). At necropsy, most of the *Pdk1*$^{fl/fl}$ mice were found to have different levels of obstruction at the proximal large intestine with a remarkable dilation of the distal small intestine as well as cecum (Figure 6Ca). Thickened rugal folds and colloid-like neoplasms in the proximal large intestine were found during gross examination, the appearance of which closely resembled that of the tumors in *Pik3ca*$^{H1047R/+}$, *Pdk1*$^{fl/fl}$ mice (Figure 6Cb). Histologically, except few cases were reported mucinous carcinoma, the rest of neoplasms of *Pdk1*$^{fl/fl}$ mice were not adenomas or carcinomas but colitis profunda or prolapse related changes, since most of them were not invasive with active inflammation, crypt abscesses or herniation of benign glands into the muscular layer

and fibrosis proliferation (Figures 6Cc,6Cd).

One notable finding was that all *Pdk1*$^{fl/fl}$ mice had a low lifetime body weight compared to their littermate controls (Figures 6D-E). The possible mechanisms behind this phenomenon include the deletion of *Pdk1* at intestinal epithelial cells leading to intestinal structural abnormalities or impairing the physiological digestion and absorption of the intestine, resulting in body weight loss. Regarding intestine structure, the length of villi at the small intestine of *Pdk1*$^{fl/fl}$ mice did not elongate as it did in oncogenic *Pik3ca* mice but was similar to the control cohort (Figure 6F). However, the length of crypts at the large intestine of *Pdk1*$^{fl/fl}$ mice was even shorter than in the control mice cohort, further confirming that the deletion of *Pdk1* at intestinal epithelial cells led to nonintact crypt formation.

The intestinal mucus coating layer is vital to maintain the physiological function of the intestine. Mucins are synthesized and then secreted by goblet cells, which are a major component of mucus and function to lubricate the epithelium and protect epithelium from damage by harmful compositions. Alcian blue staining of the intestine reveals the presence of acid mucopolysaccharide, which represents acid mucins production. In both *Pik3ca*$^{H1047R/+}$, *Pdk1*$^{fl/fl}$ and *Pdk1*$^{fl/fl}$ cohorts, the production of acid mucins were significantly reduced, which indicated deletion of *Pdk1* impaired integrity of the mucus barrier (Figures 6G, 6H). To further validate this conclusion *in vivo*, we conducted the permeability assay to monitor the barrier function of the intestine. After providing mice dextran labeled with fluorescein isothiocyanate (FITC) via gavage, FITC-dextran will be metabolized through the intestine and then can be measured in arterial blood. *Pdk1*$^{fl/fl}$ mice demonstrated the strongest FITC serum signal compared with wild-type control, demonstrating a compromised intestinal barrier in these mice primarily at the extracellular connection, possibly leading to various pathological conditions such as chronic inflammatory diseases (Figures 6I).

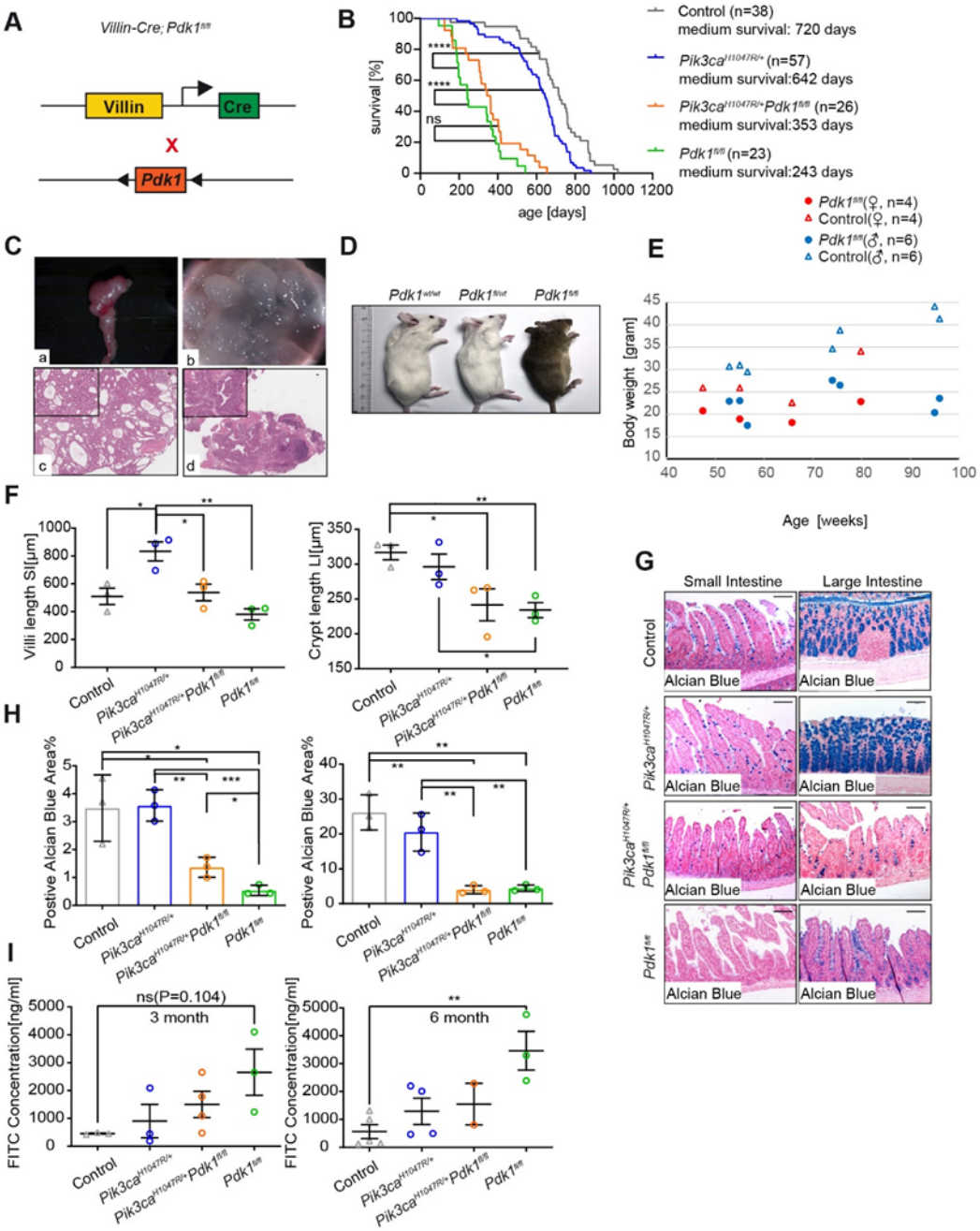

Figure 6. Ablation of *Pdk1* induces large intestine neoplasms

(A) Genetic strategy was used to block *Pdk1* expression in the intestine.

(B) Kaplan-Meier survival analysis of the indicated mouse lines. + stands for the wild-type allele (ns, not significant; ****p < 0.0001, log-rank test).

(C) Representative macroscopic (Ca/Cb), microscopic images of large intestine neoplasms from *Pdk1*$^{fl/fl}$ mice cohort. Scale bars, 100 μm.

(D) Representative images of mouse body size of the indicated genotypes.

(E) Body weight of *Pdk1*$^{fl/fl}$ end point mice and corresponding littermate control. Each circle corresponds to a *Pdk1*$^{fl/fl}$ mouse and at its same x-axis position, the triangle corresponds a littermate control.

(F) Length of the small and large intestine in *Pik3ca*$^{H1047R/+}$ mice cohort, *Pik3ca*$^{H1047R/+}$, *Pdk1*$^{fl/fl}$ mice, *Pdk1*$^{fl/fl}$ and control animals. Error bars, SEM; more than 10 villi/crypt were measured for each mouse, n=3 per group; *p < 0.1; **p < 0.01 by t test;
(G) Alcian blues staining of the intestine of indicated mice genotypes. Scale bars, 100 µm. (these assays were carried out together with Dr. Markus Tschurtschenthaler)
(H) Alcian blues analysis of the intestine of indicated mice genotypes. Error bars, SEM; n > =3 per group; Scale bars, 100 µm.
(I) FITC concentration of mice blood serum after gavage of FITC-dextran in indicated genotypes. Error bars, SEM; n>=3 per group; *p < 0.1; **p < 0.01 by t test; (these assays were carried out together with Dr. Markus Tschurtschenthaler, Regina Pietsch)

6.6. Knockin *Pdk1*$^{K465E/fl}$ mice with oncogenic *Pik3ca* only initiates malignancy at the small intestine

Pdk1 consists of two domains, a C-terminal pleckstrin homology domain, and an N-terminal kinase domain (Figure 7A). Through the C-terminal PH domain, Pdk1 interacts with phosphoinositides. To study the function of the Pdk1 PH domain in oncogenic *Pik3ca*-driven intestinal carcinogenesis, we generated a *Pdk1*$^{K465E/fl}$ mouse line, which has a point mutation at lysine 465 in exon 12 of the *Pdk1* gene instead of glutamic acid (Figure 7B). This mutation leads to a change in conformity in the PH domain of the PDK1 and thereby causes an inhibition of the binding PIP3 to PDK1, yet meanwhile, the expression of PDK1 is normal.

Kaplan-Meier survival analysis of *Pik3ca*$^{H1047R/+}$, *Pdk1*$^{K465E/fl}$ showed its median survival was approximately 514 days between the survival curves of the *Pik3ca*$^{H1047R/+}$ cohort and *Pik3ca*$^{H1047R/+}$, *Pdk1*$^{fl/fl}$ cohort (Figure 7D). In the *Pik3ca*$^{H1047R/+}$, *Pdk1*$^{K465E/fl}$ cohort, all mice developed small intestine tumors, including adenoma, cystadenoma, and carcinoma, which were identical to the tumor phenotypes in oncogenic *Pik3ca*-driven mouse model (Figures 7C). This indicates inhibition of the binding of PDK1 to PIP3 is unable to eliminate the oncogenic effect of *Pik3ca* at the small intestine. Notably, the metastasis ratio (18.2%) of all *Pik3ca*$^{H1047R/+}$, *Pdk1*$^{K465E/fl}$ mice was lower than the *Pik3ca*$^{H1047R/+}$, *Pdk1*$^{fl/fl}$ cohort, and the *Pik3ca*$^{H1047R/+}$ cohort (Figure 7E).

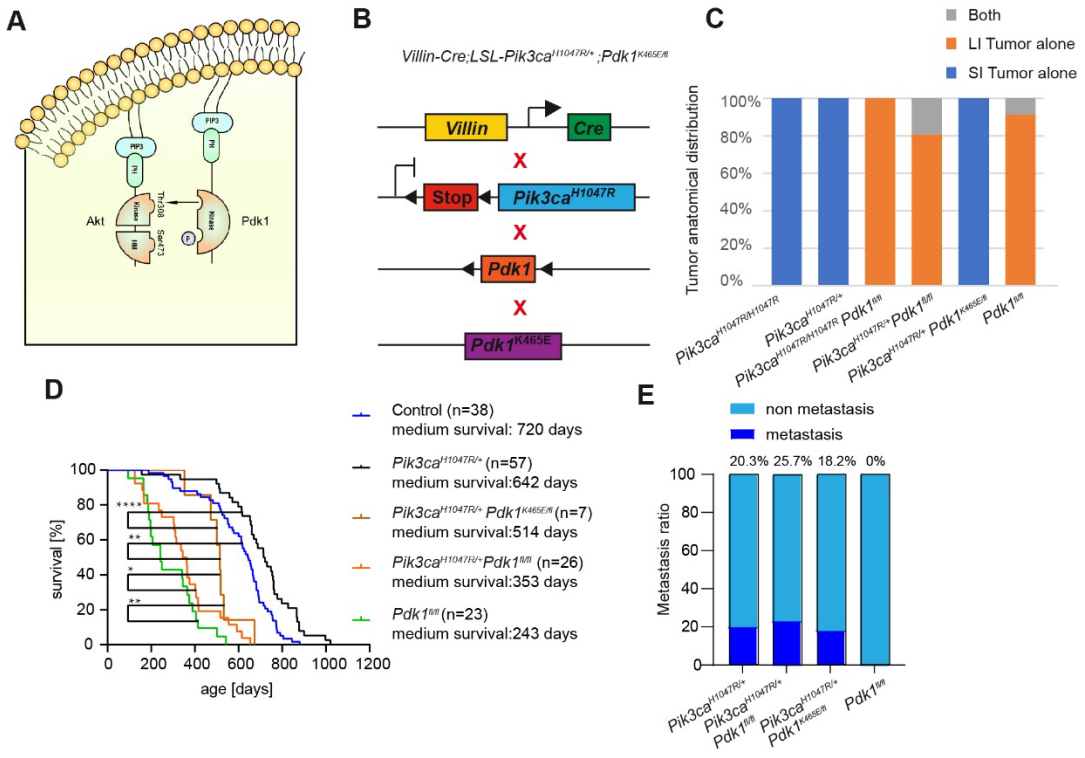

Figure 7. Knockin *Pdk1*$^{K465E/fl}$ mice with oncogenic *Pik3ca* only initiates malignancy at the small intestine

(A) Pattern diagram of Pdk1/PIP3/Akt connection.

(B) Genetic strategy used to activate *Pik3ca*^{H1047R} expression and knock in *Pdk1*$^{K465E/fl}$ in the intestine.

(C) Tumor anatomical distribution of the indicated genotypes. *Pik3ca*$^{H1047R/H1047R}$, n=17; *Pik3ca*$^{H1047R/+}$, n=57; *Pik3ca*$^{H1047R/H1047R}$, *Pdk1*$^{fl/fl}$,n=9; *Pik3ca*$^{H1047R/+}$, *Pdk1*$^{fl/fl}$, n=26; *Pik3ca*$^{H1047R/+}$, *Pdk1*$^{K465E/fl}$, n=11; *Pdk1*$^{fl/fl}$, n=26;

(D) Kaplan Meier survival analysis of the indicated mouse lines. + stands for the wild-type allele (ns, not significant; ****p < 0.0001, log-rank test).

(E) The ratio of tumor mice with metastasis in *Pik3ca*$^{H1047R/+}$, n=57; *Pik3ca*$^{H1047R/+}$, *Pdk1*$^{fl/fl}$, n=26; *Pik3ca*$^{H1047R/+}$, *Pdk1*$^{K465E/fl}$, n=11; *Pdk1*$^{fl/fl}$, n=26;

6.7. Wnt and Hippo pathways activation during *Pik3ca*-driven carcinogenesis

To examine the genetic alterations and signaling differences between duodenum tumors and non-malignant duodenum mucosa in oncogenic *Pik3ca* mice, we established an organoid biobank derived from different locations of the intestines of

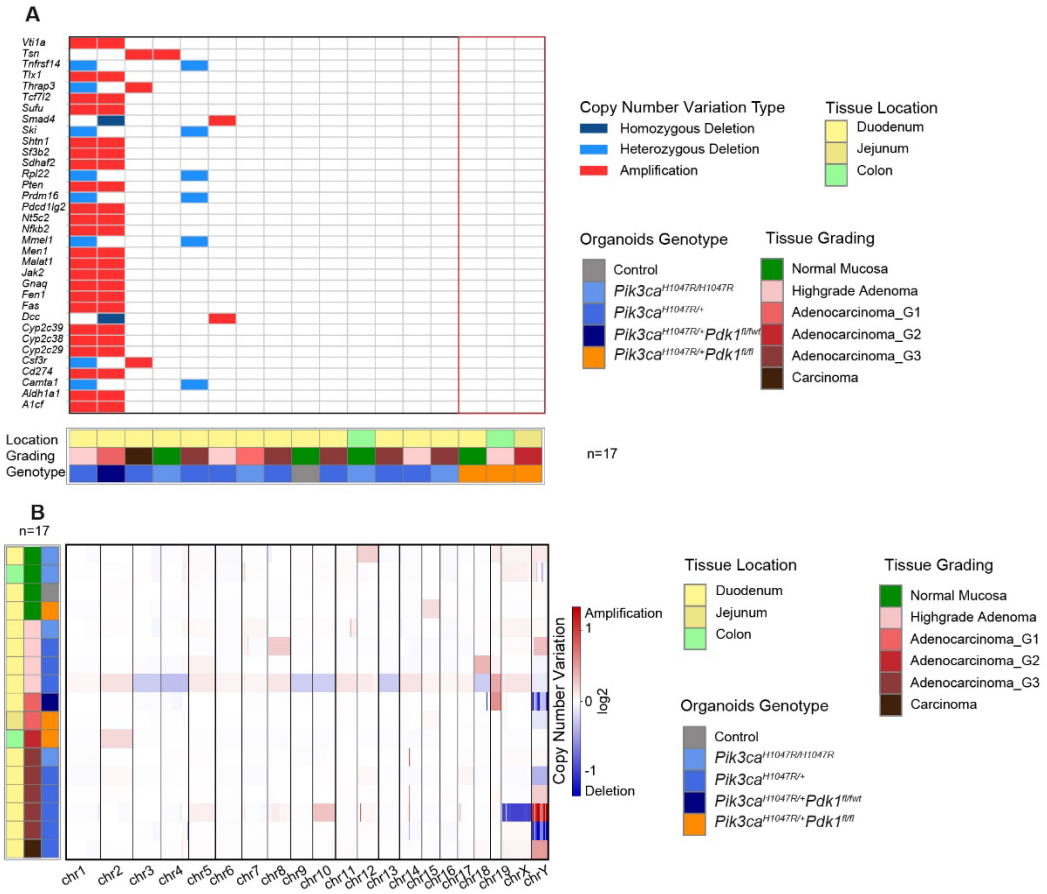

Figure 8. CNV analysis of *Pik3ca*$^{H1047R/+}$ organoids

(A) Waterfall diagram of CNV analysis indicating mutated genes (only show mutated genes were found at least twice of all samples) of organoids (n=17) from indicated genotypes and control.

(B) Landscape diagram of overview CNV analysis indicating mutated genes of organoids (n=17) from indicated genotypes and control.

genetically engineered mouse models. Copy number variation analysis showed a plethora of genetic amplifications and deletions were found in *Pik3ca* activated tumor organoids, and in *Pik3ca* activated organoids from normal mucosa, these alterations were not detected (Figure 8A). Many copy number amplifications in *Pik3ca* activated tumor organoids were related to signaling pathways such as *Sufu* (negative regulator of Hedgehog signaling) in the Hippo pathway, *Pten* (phosphatase and tensin homolog)in the PI3K pathway, and *Nfkb2* in the NFKB (nuclear factor kappa-light-chain-enhancer of activated B cells) pathway. In addition, *Vti1a*, *Dcc,* and *Cs274* variations have been reported in other studies were related to colorectal cancer. Amplification of *Tnfrsf14* and deletion of *Fas* indicated aberrant activities of TNF (tumor necrosis factor) signaling. Furthermore, the deletion of *Ski* and tumor repressor *Smad4* (mothers against decapentaplegic homolog) related to TGF-β (transforming growth

factor beta) signaling was also detected in *Pik3ca* induced tumor organoids. From the landscape overview of CNV of all samples, variations in adenocarcinoma and carcinoma did not show significant differences except for one adenocarcinoma with a higher variation frequency, this also might be not enough carcinoma samples were included (Figure 8B).

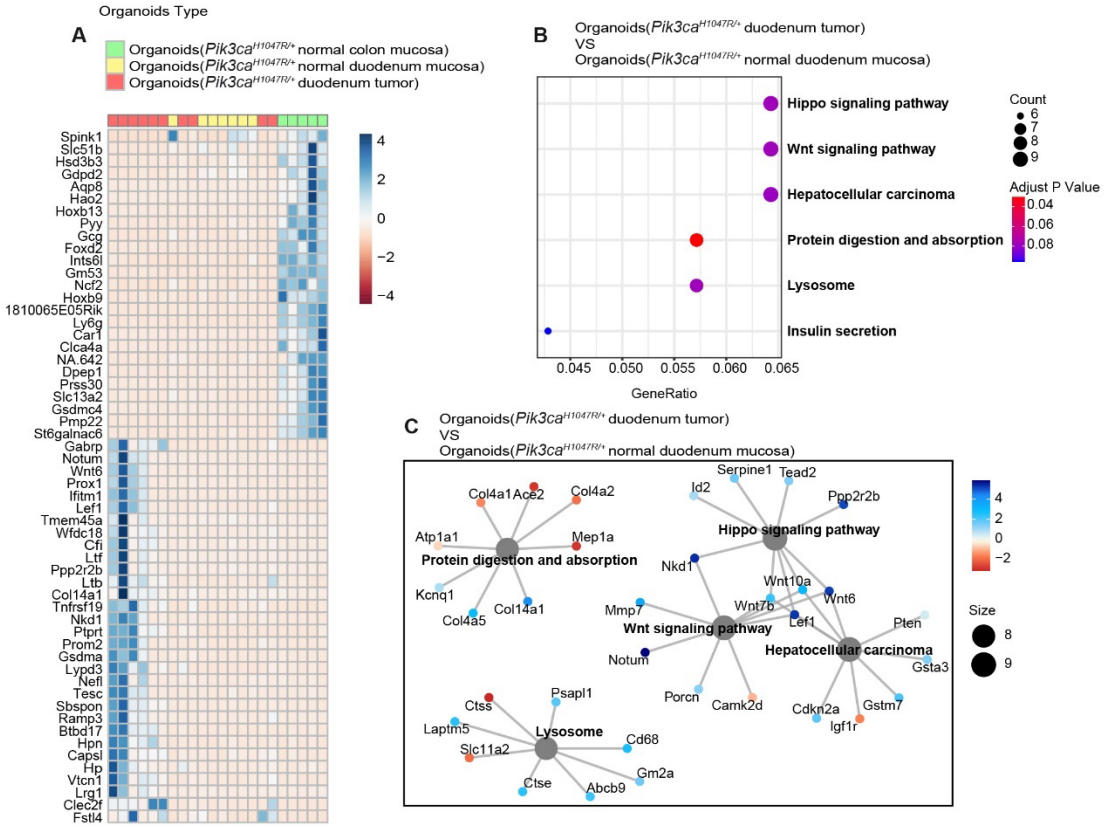

Figure 9. mRNA expression analysis of *Pik3ca*$^{H1047R/+}$ organoids

(A) Heatmap of differential mRNA expression of organoids isolated from small intestine, large intestine and tumor from *Pik3ca*$^{H1047R/+}$ mice. Differential gene expression analysis was done using edgeR and limma R packages (adjust $P < 0.05$). Red indicate under-expression genes and blue indicate over-expression genes.

(B) KEGG pathway enrichment of differential mRNA expression of *Pik3ca*$^{H1047R/+}$ duodenum tumor organoids vs *Pik3ca*$^{H1047R/+}$ duodenum organoids from normal mucosa. logFC >=4.

(C) The highest-ranked signal pathway network revealed by KEGG pathway enrichment of differential mRNA expression via cneplot R packages. Genes indicated in blue were up-downregulated in *Pik3ca*$^{H1047R/+}$ duodenum tumor organoids and the intensity of blue stands for the fold change. Genes indicated in red were up-downregulated in *Pik3ca*$^{H1047R/+}$ duodenum tumor organoids and the intensity of red stands for the fold change. Lines connecting the molecules indicate molecular relationships.

To explore the differential gene expression at the RNA level, the mRNA sequence was analyzed in organoids from duodenum tumors, and the duodenum and colon of

oncogenic *Pik3ca* mice and these three organoids groups manifested distinctly different gene expression (Figure 9A). Compared to organoids of *Pik3ca* activated small intestinal normal mucosa, expression of some transcripts related to metabolic enzymes (*Spink1*, *Slc51b*, *Hsd3b3*, *Gdpd2*, *Hao2*, *Pyy*, etc), DNA binding (*Hoxb13*, *Foxd2*), *Ly6g* expressed in immune cells and *Prss30* expressed in the distal colon were upregulated in organoids of large intestinal *Pik3ca* activated normal mucosa. Analysis of differential genes between organoids from *Pik3ca* activated small duodenum tumor versus *Pik3ca* activated duodenum showed upregulated genes in tumor organoids group were clustered in many pathways which were also found in CNV results, such as *Wnt6*, *Lef1* and *Nkd1* related to Wnt pathway, *Ptprt* involved in PAK pathway, *Tnfrsf19* in TNF pathway, *Gsdma*, *Ptprt* and *Fstl4* involved in colorectal cancer. Further enrichment analysis of significant differential genes indicated Wnt and Hippo pathways were notably increased in duodenum tumors compared with duodenum organoids from *Pik3ca* mice, also the activities of lysosome and protein digestion and absorption (Figures 9B,9C).

6.8. Oncogenic *Pik3ca* accelerates proliferation *in vitro*

The challenge of propagating cell lines from intestinal epithelium has hindered studies into the molecular and cellular mechanisms behind the various intestinal cell lineages. Specifically, there are a dearth of long-term cultures of epithelial cell from the intestine, although some short-term epithelial cell culture method have been reported. To overcome this problem, organoid cultures, a three-dimensional (3D) tissues, were applied to examine long-term intestinal epithelial cell cultures *in vitro* as they consist of physiologically related characteristics of intestinal tissue *in vivo*, such as polarized epithelial layers next lumens, different cell types of the intestinal epithelium (Figure 10A).

We successfully cultured duodenum, colon, and tumor organoids from the engineered mice genotypes and established an intestinal organoids biobank. However, *Pdk1*

deletion organoids including organoids from normal intestine of *Pik3ca*$^{H1047R/+}$, *Pdk1*$^{fl/fl}$ mice and *Pdk1*$^{fl/fl}$ mice encountered growth arrest and were not able to proceed long-term culture *in vitro*. To examine the proliferation status in specific organoid lines, we monitored Ki67 positive cells. We found the ratio of the positive cells was approximately 10% in duodenum and colon organoids derived from control mice and *Pik3ca*$^{H1047R/+}$, *Pdk1*$^{fl/fl}$ mice (Figures 10B,10D). Normal mucosa organoids from *Pik3ca*$^{H1047R/+}$ mice showed a higher proliferation rate, which was consistent with our results *in vivo*. As expected, *Pdk1*$^{fl/fl}$ organoids demonstrated a lower amount of Ki67 positive cells amount, further implying that PDK1 is vital to maintain growth and proliferation. Of note, organoids from tumors of *Pik3ca*$^{H1047R/+}$ and *Pik3ca*$^{H1047R/+}$, *Pdk1*$^{fl/fl}$ mice demonstrated remarkably increased Ki67 positive cells, almost approximately 50%. Interestingly, duodenum and colon organoids from normal mucosa of *Apc* $^{fl/wt}$, *Pdk1*$^{fl/fl}$ represented abnormal proliferation, indicating even partial loss of Apc could reverse the inhibition of proliferation due to deletion of *Pdk1*.

Furthermore, to determine alterations of ERK signaling, we texted the level of p-ERK1/2 of endogenous organoids and inducible *Pdk1*$^{fl/fl}$ organoids after 1, 2, and 3 days of tamoxifen treatment (Figures 10C,10F). The p-ERK1/2 in organoids of the SI and LI in *Pik3ca*$^{H1047R/+}$ mice was activated relative to the control *in vitro* culture, but not *Pik3ca*$^{H1047R/+}$ tumor organoids, indicating activation of p-ERK1/2 *in vivo* was not positively connected with *Pik3ca*^{H1047R}-driven tumors (Figure 10E). In organoids from *Pik3ca*$^{H1047R/+}$, *Pdk1*$^{fl/fl}$ mice, duodenum, colon and tumor groups showed a uniform level of p-ERK1/2. However, organoids from the deletion of *Pdk1*$^{fl/fl}$ mice displayed a lower level of p-ERK1/2, which was opposite with that increased p-ERK1/2 in vivo *Pdk1* ablation models. As for tamoxifen treatment timepoint assay on *CreER*^{T2}, *Pdk1*$^{fl/fl}$ organoids, the aim was to gradually delete *Pdk1 in vitro* and examine the corresponding p-ERK1/2 changes (Figures 10F,10G). And the IHC data demonstrated that p-ERK1/2 was only not detectable in duodenum organoids from *CreER*^{T2}, *Pdk1*$^{fl/fl}$ on day1 treatment and the rest of groups did not exhibit literally changes. All these

imply aberrant ERK1/2 *in vivo* intestine in our GEMM was affected by extrinsic microenvironment rather than intrinsic signaling cascades driven by *Pik3ca* or *Pdk1* genetic alterations.

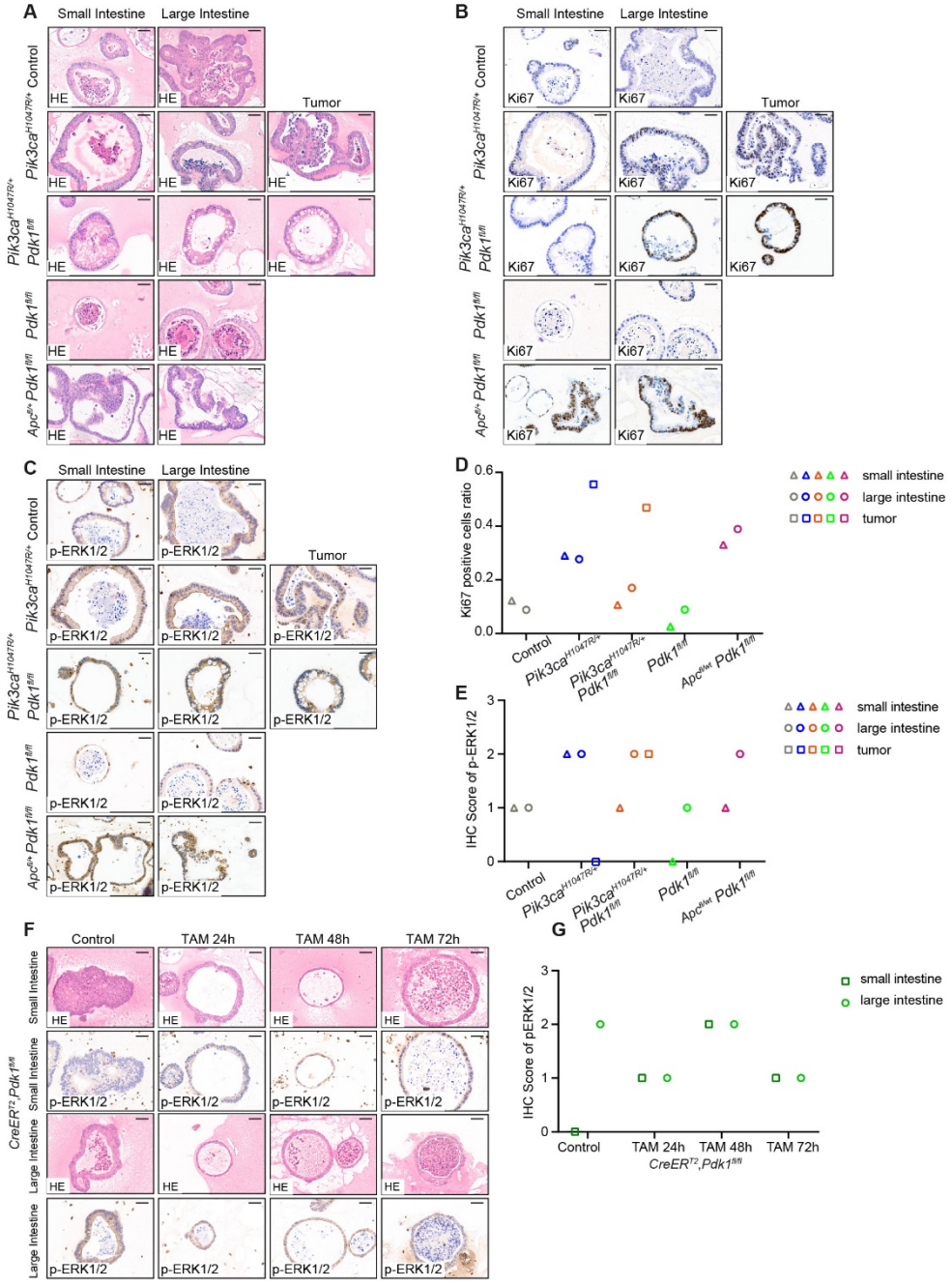

Figure 10. Oncogenic *Pik3ca* accelerates proliferation in vitro

(A) Representative microscopic images of HE staining of organoids from indicated genotypes. Scale bars, 100 µm.

(B) Representative microscopic images of Ki67 staining of organoids from indicated genotypes. Scale bars, 100 µm.

(C) Representative microscopic images of p-ERK1/2 (p-p44/p42MAPK) staining of organoids from indicated genotypes. Scale bars, 100 μm.
(D) Quantification of positive cells by Ki67 staining of organoids from indicated genotypes. n >=3 per group.
(E) Quantification of IHC score of p-ERK1/2 staining of organoids from indicated genotypes. n >=3 per group.
(F) Representative microscopic images of organoids from *Cre-ER*^{T2} ,*Pdk1*$^{fl/fl}$ at different tamoxifen treatment timepoint. Scale bars, 100 μm.
(G) Quantification of IHC score of p-ERK1/2 staining of organoids with from Cre-ER^{T2} ,Pdk1$^{fl/fl}$ at different tamoxifen treatment timepoint. n >=3 per group.

6.9. Ablation of *Pdk1* in vitro impair growth

To overcome conundrum of growth disadvantages of endogenous intestinal organoids from *Pdk1*$^{fl/fl}$ mice, we relied on an inducible organoids system. We isolated organoids from *CreER*^{T2}, *Pdk1*$^{fl/fl}$ mice with GFP (the green fluorescent protein) /tdTomato reporter, and subjected them to 3 days of tamoxifen treatment to delete PDK1 *in vitro* (Figure 11A). The untreated organoids manifested tdTomato red signal and the tamoxifen-treated ones switched to green GFP signals. Recombined PCR of *Pdk1* showed after 3 days of tamoxifen treatment, *Pdk1* was successfully deleted in both small intestine and large intestine group (Figures 11B-11F). However, the *Pdk1* deficiency organoids cannot be cultured for the long term, as the green signal gradually reduces after several passages. This implied that mutant *Pdk1* signals exhibited advantages of growth and loss of *Pdk1* impeded organoid growth in both small intestine and large intestine groups (Figures 11G-11J).

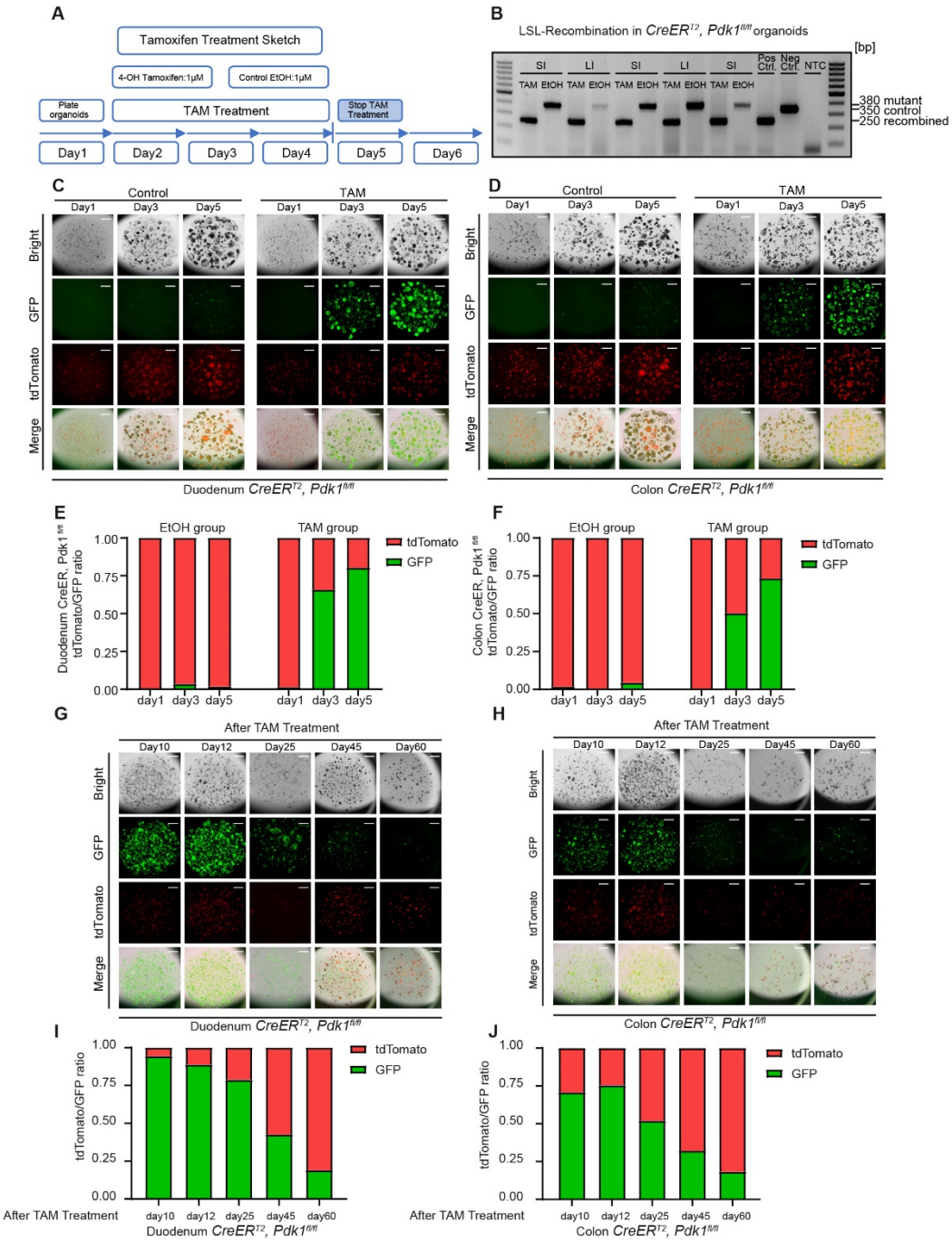

Figure 11. Ablation of *Pdk1* in vitro impair growth

(A) Tamoxifen treatment sketch of *Cre-ER*^{T2} ,*Pdk1*$^{fl/fl}$ intestinal organoids.

(B) Recombination PCR of tamoxifen-induced *Cre-ER*^{T2} ,*Pdk1*$^{fl/fl}$ organoids. (DNA of organoids was harvested at the day 6). Small intestine (SI); Large intestine (LI) ; Control (Ctrl); NTC (No template control)

(C) Representative microscopic images of *Cre-ER*^{T2} ,*Pdk1*$^{fl/fl}$ small intestine organoids at day1, day3 and day5. Scale bars, 100 µm. n>=10 per group.

(D) Representative microscopic images of *Cre-ER*^{T2} ,*Pdk1*$^{fl/fl}$ large intestine organoids at day1, day3 and day5. Scale bars, 100 µm. n>=10 per group.

(E) Quantification of fluorescent intensity of *Cre-ER*^{T2} ,*Pdk1*$^{fl/fl}$ small intestine organoids at day1, day3 and day5.

(F) Quantification of fluorescent intensity of *Cre-ER*^{T2} ,*Pdk1*$^{fl/fl}$ large intestine organoids at day1, day3 and day5.
(G) Representative microscopic images of *Cre-ER*^{T2} ,*Pdk1*$^{fl/fl}$ small intestine organoids at day10, day12, day25, day 45 and day60. Scale bars, 100 μm. n>=10 per group.
(H) Representative microscopic images of *Cre-ER*^{T2} ,*Pdk1*$^{fl/fl}$ large intestine organoids at day10, day12, day25, day 45 and day60. Scale bars, 100 μm. n>=10 per group.
(I) Quantification of fluorescent intensity of *Cre-ER*^{T2} ,*Pdk1*$^{fl/fl}$ small intestine organoids at day10, day12, day25, day 45 and day60.
(J) Quantification of fluorescent intensity of *Cre-ER*^{T2} ,*Pdk1*$^{fl/fl}$ large intestine organoids at day10, day12, day25, day 45 and day60.

7. Discussion and outlook

Role of *Pdk*1 in CRC progression and metastasis

PI3K signaling is linked to downstream activation of PDK1, AKT, mTORC1 and TEC (tyrosine-protein kinase Tec) kinases, and GEFs (guanine nucleotide exchange factors) /GAPs for GTPases (Fernandes, Sanches, & Seruca, 2018; Narayanankutty, 2019; Slattery et al., 2018). PDK1 is one of the key effectors triggered by oncogenic *Pik3ca*^{H1047R}, which is connected to proliferation, metabolism, differentiation, and apoptosis (Gagliardi, Puliafito, & Primo, 2018; Niba et al., 2013). In our data, the protein level of Pdk1 was found to increase in the intestine of *Pik3ca*^{H1047R} mice, and ablation of *Pdk1* in *Pik3ca*^{H1047R}-driven mouse models did block CRC formation in the SI but did not initiate neoplasms in the LI. This implies *Pdk1* is essential for small intestine tumorigenesis in *Pik3ca*^{H1047R}-driven mice, and thus *Pdk1* could be further investigated as a potential target for CRC therapy. However, the deletion of *Pdk1* induced neoplasms in the large intestine and cecum and led to growth retardation and intestinal dysfunction *in vivo* in the mouse model. In addition, organoids derived from *Pdk1*$^{fl/fl}$ mice can only be cultured *in vitro* in the presence of mosaic mutant *Pdk1*. In our tamoxifen-inducible *in vitro* model, the deletion of *Pdk1* was resistant and displayed significant growth disadvantages. This work demonstrated the deletion of *Pdk1* contributes to the inhibition of tumor formation in the small intestine, while the ablation of *Pdk1* suppresses cell growth and proliferation intensely and leads to disrupted crypt homeostasis. Thus, a certain endogenous level of PDK1 is also essential for mice development and intestinal function. This conclusion also was supported by other studies that inhibition of PDK1 in colon cell lines via RNAi could suppress cell growth and induce apoptosis (Lawlor et al., 2002; Lu, Cox-Hipkin, Windsor, & Boyapati, 2010).

The elimination of *Pdk1* in oncogenic mice only slightly reduced the metastasis occurrence from 18% metastasis cases in *Pik3ca*$^{H1047R/+}$ tumor mice cohort to 11% in *Pik3ca*$^{H1047R/+}$, *Pdk1*$^{fl/fl}$ tumor mice cohort. In *Pdk1*$^{fl/fl}$ mice cohort, no metastatic lesions

were found during the gross sections. This elucidates deletion *Pdk1* does not facilitate the occurrence of metastasis induced by oncogenic *Pik3ca*, yet shows a subtle inhibition effect on metastasis driven by oncogenic *Pik3ca*. In one review from Gagliardi et al., they concluded AKT, intergrin β3, PAK1, PLCγ1 (phosphoinositide phospholipase C gamma 1), MRCKα and ROCK1 might particpate in PDK1 regulated cell migration and via invadopodia formation and amoeboid, PDK1 also contributes to tumor cell invasion (Gagliardi, di Blasio, & Primo, 2015).

In future experiments, global transcriptome, phospho-proteome, and supernatant proteome analyses will be performed for tamoxifen-induced *Pdk1*-deleted organoids and tamoxifen-induced *Pik3ca*-mutant organoids to identify potential effectors and key mechanisms, cross-talk to other related pathways, e.g., ERK signaling, mTOR signaling, DNA damage response and senescence, etc.

Aberrant growth retardation of *Pdk1$^{fl/fl}$* mice is connected with metabolism and adipocytes changes

In our *Pdk1$^{fl/fl}$* genetic mouse model, all mice displayed abnormal low body weight, intact intestinal function, and aberrant levels of serum glucose. One mechanism behind this might be that the ablation of *Pdk1* interfered with the metabolism of intestinal cells and lipid production. In research of Li et al., metabolic profiles of cardiomyocytes in mice with a *Pdk1* deletion showed significantly enhanced levels of glutamine, acetate, glutamate, and O-phosphocholine and significantly decreased levels of glycine, lactate, alanine, fumarate, choline, taurine, IMP (inosine 5'-monophosphate), AMP (adenosine monophosphate), and ATP (adenosine triphosphate) compared to controls (C. Li et al., 2019). These findings imply *Pdk1* deletion makes a substantial difference in mouse metabolic activities. Another study reported in vascular endothelial *Pdk1* knock-out mice that ablation of *Pdk1 in vivo* not only intervened with the production of adipose tissue but also leads to enhanced energy disbursement due to the amelioration of adipocytokine profiles (Tawaramoto et al., 2012). This study supports the evidence of

an unexpected role of *Pdk1* in endothelial cells on the stabilization of proper glucose homeostasis via the ordinance of adipocyte development. These findings inspire us to investigate further the effect of *Pdk1* on metabolism profiles of intestinal epithelial cells and adipocytes of the intestine in our *Pdk1*$^{fl/fl}$ genetic mouse model.

Resistance towards PDK1 inhibition

In this study, *Pdk1* was validated to play a dual role in intestinal carcinogenesis via characterization of *Pik3ca*$^{H1047R/+}$ mice and *Pik3ca*$^{H1047R/+}$, *Pdk1*$^{fl/fl}$ mice. By using a *Pik3ca*$^{H1047R/+}$, *Pdk1*$^{fl/fl}$ model to genetically eliminate *Pdk1*, the small intestinal tumorigenesis driven by oncogenic *Pik3ca* was suppressed while metabolism changes and unbalanced crypt homeostasis induced by inactivation of *Pdk1* triggered mucinous adenocarcinoma at the large intestine. To test the role of *Pdk1* at intestinal epithelial cells, *Pdk1*$^{fl/fl}$ mice cohort was generated to establish *Pdk1*$^{fl/fl}$ organoids bank. However, *Pdk1*$^{fl/fl}$ intestinal organoids were not able to be cultured in LWRN medium, and few *Pdk1*$^{fl/fl}$ *Pdk1*$^{fl/fl}$ intestinal organoids showed mutant *Pdk1* band after PCR. This is probably due to the impaired AKT signaling or insufficient other indispensable factors for organoids growth. To overcome endogenous mosaic *Pdk1*$^{fl/fl}$ effects, an inducible *CreER*$^{T2/+}$, *Pdk1*$^{fl/fl}$ system with tdTomato/GFP reporter was applied to detect the level of RNA/protein expression and signaling alterations after the ablation of *Pdk1*. Upon 3-day tamoxifen treatment, *Pdk1* was deleted but organoids were not able to maintain the growth and proliferation. The growth of few mutant *Pdk1* organoids gradually surpassed the growth of the *Pdk1* deleted organoids during the long-time culture. This hints on the genetic *Pdk1* ablation harbouring the disadvantage of resistance.

Some researches demonstrated the PDK1 inhibitors were not effective *in vivo*. For instance, were reported as compounds inhibiting PDK1 selectively while BX-795, one type of aminopyrimidines, was validated to suppress also other enzymes like TANK-binding kinase 1 (TBK1) and ERK8 (Bain et al., 2007). Another novel PDK1 inhibitor GSK2334470 was reported inhibiting PDK1 activity, however S6K signaling was

decreased more strongly than AKT signaling at the same concentration, indicating variability in PDK1 inhibitor GSK2334470 (Najafov, Sommer, Axten, Deyoung, & Alessi, 2011). Therefore, it would be interesting to treat *Villin-Flp, FSF-Pik3ca$^{H1047R/+}$, Cre-ER^{T2}, Pdk1$^{fl/fl}$* mice with GSK2334470 to compare the outcome to the genetic *Pdk1* ablation by tamoxifen.

Pik3ca$^{H1047R/+}$,_Pdk1_$^{fl/fl}$ mice can be a model for appendiceal mucinous neoplasm

In our *Pik3ca$^{H1047R/+}$,Pdk1$^{fl/fl}$* genetic mouse model, appendiceal and proximal colonic mucinous neoplasms were found with pathological features of mucin-filled, cystically dilated tissue. The appendiceal and proximal colonic wall around neoplasm tissue usually appears fibrotic, hyalinized, stiff with a smooth or granular appearance. This mucinous neoplasm phenotype is identical to human appendiceal mucinous neoplasm (AMN), which is a rare malignancy with diverse clinical symptoms depending on the manifestation (Campbell, 1981). AMN has been described in several studies and is usually associated with an array of dissections, diverticula, herniations, and rupture disease (Panarelli & Yantiss, 2011; Tirumani et al., 2013; Yu et al., 2020). A standardized clinical treatment approach is not systemically established, yet an appendectomy approach is recommended for the resection of non-metastatic disease according to some case reports. These studies found AMN in humans harboring Kras and CEA genetic alterations (Hara et al., 2015). Our mouse study offers a potential mechanism for AMN carcinogenesis: the deletion of *Pdk1* at intestinal epithelial cells interrupts crypt homeostasis and intestine dysfunction resulting in mucinous neoplasms. The *Pik3ca$^{H1047R/+}$,Pdk1$^{fl/fl}$* genetic mouse model also offers the opportunity to investigate AMN via mice research *in vivo*.

Difference between SI and LI crypt homeostasis

In our mouse model characterization, small intestine and large intestine of mice manifest a discrepancy in anatomical structures that corresponds with their distinct physiological function. The finger-shaped villi are present in the SI while not in the LI

to increase surface area to absorb maximum nutrients (Shafik, El-Sibai, & Ahmed, 2001; Sheppard & Sterns, 1975). The function of the large intestine is to absorb water and fermentation, and the mucus layer of the large intestine is approximately four-fold thicker than that of the upper part of the small intestine. In addition, immune cell subtypes and microbiota populations are also different in the small intestine and large intestine, which interact with their unique function and structure. The small intestine of the *Pik3ca*^{H1047R} mouse model demonstrated longer intestine length and obvious elongation of villi, while in the large intestine, higher mucin production was found. Furthermore, increased BrdU positive cells in the crypt niche were detected in both the small and large intestine. These alterations imply intestinal epithelial hemostasis in the *Pik3ca*^{H1047R} mouse model is interrupted that crypt niche tends to be hyperproliferative. Intestinal epithelial hemostasis is critical to sustaining the physiological function and structure of the intestine, the epithelial lining of which intestinal harbors rapidly renewing cell populations (Du, Nie, & Holmes, 2015; Smith, Rao-Bhatia, & Kim, 2017; Snippert et al., 2010).

Role of *ERK1/2* in *Pik3ca*^{H1047R}-driven CRC

Apart from PDK1, the level of ERK1/2 of the MAPK superfamily was also subtle upregulated in the large intestine of oncogenic *Pik3ca* mice. Once genetically deleted *Pdk1*, the level of ERK1/2 was remarkablely increased in both the small intestine and the large intestine. However, the activation of ERK1/2 was only validated *in vivo* mice and the genetical ablation of *Pdk1* organoids *in vitro* did not show the increase in the level of ERK1/2. Besides, RNA sequence data about oncogenic *Pik3ca* induced tumor organoids indicated ERK1/2 was not significantly involved and changed in *Pik3ca*^{H1047R} tumor organoids compared to *Pik3ca*^{H1047R} organoids from normal small intestine mucosa *in vitro*. No notable alterations in MAPK signaling were detected according to our copy number variation analysis *of Pik3ca*^{H1047R} tumor organoids. Taken together, our results manifested the increased level of ERK1/2 was not aroused by signaling alteration cascades induced by oncogenic *Pik3ca* and /or ablation of *Pdk1*, yet might

be a consequence of extrinsic microenvironment changes. To validate this result in vivo, we tried to generate a mouse line to simultaneous inactivate *ERK1/2* based on oncogenic *Pik3ca* mouse model. Unfortunately, homozygous deletion of *ERK1/2* in a mouse model is lethal and in heterozygous *Pik3ca*$^{H1047R/+}$, *ERK1*$^{fl/wt}$, *ERK2*$^{fl/fl}$ mice and *Pik3ca*$^{H1047R/+}$, *ERK1*$^{fl/fl}$, *ERK2*$^{fl/wt}$ mice, the tumor initiation at the small intestine, overall survival and tumor phenotypes were identical with *Pik3ca*$^{H1047R/+}$ mice (data was not shown). Besides, Erk signaling was also reported as an indispensable pathway for self-renewal and genomic stability of murine embryonic stem cells and conditional block of ERK1/2 led to murine delayed parturition and abnormal placentation (Brown et al., 2019; Chen et al., 2015). These observations extend our previous results that partial inactivation of *ERK1/2* was not enough to repress oncogenic Pik3ca-driven small intestine carcinogenesis. One approach that can be carried out in the next step is to use MAPK inhibitors on *Pik3ca*$^{H1047R/+}$ organoids to validate whether reduced MAPK signaling is a potential target to impair *Pik3ca*$^{H1047R/+}$-induced intestinal tumors growth.

Conclusion

To summarize, this study looks into the role of PI3K/ PDK1 signaling in carcinogenesis of intestinal cancer in *Pik3ca*^{H1047R}-driven mouse models. Oncogenic *Pik3ca* was able to initiate adenoma and metastatic adenocarcinoma with increased level of PDK1, Wnt and Hippo signaling. PDK1 was shown to be important for intestinal proliferation, crypt homeostasis, metabolism *in vivo*. However, a subpopulation of organoids was capable to survive genetic *Pdk1* deletion and giving rise to resistant organoids. Further researches will be needed to evaluate PDK1 as a promising therapeutic target in CRC aiming at alleviating this malignant disease and overcome resistance.

Acknowledge conflicts

In this project, some experiments and mouse lines were shared with other members in AG Saur lab, especially Dr. Markus Tschurtschenthaler and Regina Pietsch. Regina

Pietsch established *Pik3ca*^{H1047R} and *Pdk1*$^{fl/fl}$ mouse lines and contributed to fundamental work for this project. *Pik3ca*^{H1047R} mouse line characterization in detail will be presented in the unpublished doctoral thesis of Regina Pietsch. All survival curves in this thesis include animals from Meng Lei, Regina Pietsch, and Markus Tschurtschenthaler and ,data were shared. Analytical data were done by Meng Lei except for CNV together with Yuexin Chen and Anantharamanan Rajamani, WES analysis together with Anantharamanan Rajamani, RNA sequence together with Yuexin Chen and Xiaoxiao Zhang.

Acknowledgements

First of all, I would like to thank everyone who contributed to this M.D thesis.

Above all, I thank Prof. Dr. Dieter Saur for giving me the opportunity to peform this promising project, for his valuable comments and support on the project, and revision of the thesis.

I’m also thankful to PD Dr. Günter Schneider for being a member of my MD committee.

Furthermore, I owe my gratitude to Yuexin Chen for bioinformatical analysis of RNA sequencing and CNV sequencing data and Fabio Boniolo for offering pipelines of RNA sequencing. Anantharamanan Rajamani for bioinformatical analysis of CNV sequencing data and WES analysis. Tania Santos and Dr. MarkusTschurtschenthaler for diligent revision of the thesis. Lujia Zhang, Ruth Schulte, Mirjam Goeth for kindly revising the abstract in Germany. Dr. Moritz Jesinghaus for professional pathological analysis. Markus Raspe and Magda Zukowska for excellent technical support. Dr. MarkusTschurtschenthaler and Regina Pietsch for establishing mouse lines, and previous fundamental work. Joanna Madej, Tania Santos, and Tatiana Martins for helping experimental techniques and kindly support. All animal caretakers for caring for the mice. All other colleagues for the nice atmosphere in the lab. Above all, the Chinese Scholarship Council for financial support during my doctoral study.

Finally, I want to thank all my family and friends for their support and help.

References

Agazie, Y. M., & Hayman, M. J. (2003). Molecular mechanism for a role of SHP2 in epidermal growth factor receptor signaling. *Mol Cell Biol, 23*(21), 7875-7886. doi:10.1128/mcb.23.21.7875-7886.2003

Anderson, E. J., Mollon, L. E., Dean, J. L., Warholak, T. L., Aizer, A., Platt, E. A., . . . Davis, L. E. (2020). A Systematic Review of the Prevalence and Diagnostic Workup of PIK3CA Mutations in HR+/HER2- Metastatic Breast Cancer. *Int J Breast Cancer, 2020*, 3759179. doi:10.1155/2020/3759179

Armaghany, T., Wilson, J. D., Chu, Q., & Mills, G. (2012). Genetic alterations in colorectal cancer. *Gastrointest Cancer Res, 5*(1), 19-27.

Arsenic, R. (2014). Immunohistochemical analysis of PDK1 expression in breast cancer. *Diagn Pathol, 9*, 82. doi:10.1186/1746-1596-9-82

Bain, J., Plater, L., Elliott, M., Shpiro, N., Hastie, C. J., McLauchlan, H., . . . Cohen, P. (2007). The selectivity of protein kinase inhibitors: a further update. *Biochem J, 408*(3), 297-315. doi:10.1042/BJ20070797

Bayascas, J. R., Wullschleger, S., Sakamoto, K., Garcia-Martinez, J. M., Clacher, C., Komander, D., . . . Alessi, D. R. (2008). Mutation of the PDK1 PH domain inhibits protein kinase B/Akt, leading to small size and insulin resistance. *Mol Cell Biol, 28*(10), 3258-3272. doi:10.1128/MCB.02032-07

Bian, X., Gao, J., Luo, F., Rui, C., Zheng, T., Wang, D., . . . Cheng, H. (2018). PTEN deficiency sensitizes endometrioid endometrial cancer to compound PARP-PI3K inhibition but not PARP inhibition as monotherapy. *Oncogene, 37*(3), 341-351. doi:10.1038/onc.2017.326

Biondi, R. M., Komander, D., Thomas, C. C., Lizcano, J. M., Deak, M., Alessi, D. R., & van Aalten, D. M. (2002). High resolution crystal structure of the human PDK1 catalytic domain defines the regulatory phosphopeptide docking site. *EMBO J, 21*(16), 4219-4228. doi:10.1093/emboj/cdf437

Boivin, G. P., Washington, K., Yang, K., Ward, J. M., Pretlow, T. P., Russell, R., . . . Coffey, R. J. (2003). Pathology of mouse models of intestinal cancer: consensus report and recommendations. *Gastroenterology, 124*(3), 762-777. doi:10.1053/gast.2003.50094

Borowsky, J., Dumenil, T., Bettington, M., Pearson, S. A., Bond, C., Fennell, L., . . . Whitehall, V. (2018). The role of APC in WNT pathway activation in serrated neoplasia. *Mod Pathol, 31*(3), 495-504. doi:10.1038/modpathol.2017.150

Braunstein, E. M., Qiao, X. T., Madison, B., Pinson, K., Dunbar, L., & Gumucio, D. L. (2002). Villin: A marker for development of the epithelial pyloric border. *Dev Dyn, 224*(1), 90-102. doi:10.1002/dvdy.10091

Bray, F., Ferlay, J., Soerjomataram, I., Siegel, R. L., Torre, L. A., & Jemal, A. (2018). Global cancer statistics 2018: GLOBOCAN estimates of incidence and mortality worldwide for 36 cancers in 185 countries. *CA Cancer J Clin, 68*(6), 394-424. doi:10.3322/caac.21492

Brouwer, N. P. M., Bos, A., Lemmens, V., Tanis, P. J., Hugen, N., Nagtegaal, I. D., . . . Verhoeven, R. H. A. (2018). An overview of 25 years of incidence, treatment and outcome of colorectal cancer patients. *Int J Cancer, 143*(11), 2758-2766. doi:10.1002/ijc.31785

Brown, J. L., Sones, J. L., Angulo, C. N., Abbott, K., Miller, A. D., Boehm, U., & Roberson, M. S. (2019). Conditional loss of ERK1 and ERK2 results in abnormal placentation and delayed parturition in the mouse. *Sci Rep, 9*(1), 9641. doi:10.1038/s41598-019-45997-0

Brunet, A., Park, J., Tran, H., Hu, L. S., Hemmings, B. A., & Greenberg, M. E. (2001). Protein kinase SGK mediates survival signals by phosphorylating the forkhead transcription factor FKHRL1 (FOXO3a). *Mol Cell Biol, 21*(3), 952-965. doi:10.1128/MCB.21.3.952-965.2001

Calistri, D., Rengucci, C., Seymour, I., Leonardi, E., Truini, M., Malacarne, D., . . . Giaretti, W. (2006). KRAS, p53 and BRAF gene mutations and aneuploidy in sporadic colorectal cancer progression. *Cell Oncol, 28*(4), 161-166. doi:10.1155/2006/465050

Campbell, T. E. (1981). Mucinous neoplasms of the appendix appearing as hernias. *Arch Pathol Lab Med, 105*(1), 57-58.

Casamayor, A., Morrice, N. A., & Alessi, D. R. (1999). Phosphorylation of Ser-241 is essential for the activity of 3-phosphoinositide-dependent protein kinase-1: identification of five sites of phosphorylation in vivo. *Biochem J, 342 (Pt 2)*, 287-292.

Castellano, E., & Downward, J. (2011). RAS Interaction with PI3K: More Than Just Another Effector Pathway. *Genes Cancer, 2*(3), 261-274. doi:10.1177/1947601911408079

Chang, D. Z., & Abbruzzese, J. L. (2005). Capecitabine plus oxaliplatin vs infusional 5-fluorouracil plus oxaliplatin in the treatment of colorectal cancer. Pro: The CapeOx regimen is preferred over FOLFOX. *Clin Adv Hematol Oncol, 3*(5), 400-404.

Chappell, W. H., Steelman, L. S., Long, J. M., Kempf, R. C., Abrams, S. L., Franklin, R. A., . . . McCubrey, J. A. (2011). Ras/Raf/MEK/ERK and PI3K/PTEN/Akt/mTOR inhibitors: rationale and importance to inhibiting these pathways in human health. *Oncotarget, 2*(3), 135-164. doi:10.18632/oncotarget.240

Chen, H., Guo, R., Zhang, Q., Guo, H., Yang, M., Wu, Z., . . . Chen, L. (2015). Erk signaling is indispensable for genomic stability and self-renewal of mouse embryonic stem cells. *Proc Natl Acad Sci U S A, 112*(44), E5936-5943. doi:10.1073/pnas.1516319112

Collins, B. J., Deak, M., Arthur, J. S., Armit, L. J., & Alessi, D. R. (2003). In vivo role of the PIF-binding docking site of PDK1 defined by knock-in mutation. *EMBO J, 22*(16), 4202-4211. doi:10.1093/emboj/cdg407

Crockett, S. D., & Nagtegaal, I. D. (2019). Terminology, Molecular Features, Epidemiology, and Management of Serrated Colorectal Neoplasia. *Gastroenterology, 157*(4), 949-966 e944. doi:10.1053/j.gastro.2019.06.041

Danese, E., Minicozzi, A. M., Benati, M., Montagnana, M., Paviati, E., Salvagno, G. L., . . . Guidi, G. C. (2015). Comparison of genetic and epigenetic alterations of primary tumors and matched plasma samples in patients with colorectal cancer. *PLoS One, 10*(5), e0126417. doi:10.1371/journal.pone.0126417

De Palma, F. D. E., D'Argenio, V., Pol, J., Kroemer, G., Maiuri, M. C., & Salvatore, F. (2019). The Molecular Hallmarks of the Serrated Pathway in Colorectal Cancer. *Cancers (Basel), 11*(7). doi:10.3390/cancers11071017

di Blasio, L., Gagliardi, P. A., Puliafito, A., Sessa, R., Seano, G., Bussolino, F., & Primo, L. (2015). PDK1 regulates focal adhesion disassembly by modulating endocytosis of alphavbeta3 integrin. *J Cell Sci, 128*(5), 863-877. doi:10.1242/jcs.149294

Dieterle, A. M., Bohler, P., Keppeler, H., Alers, S., Berleth, N., Driessen, S., . . . Stork, B. (2014). PDK1 controls upstream PI3K expression and PIP3 generation. *Oncogene, 33*(23), 3043-3053. doi:10.1038/onc.2013.266

Du, H., Nie, Q., & Holmes, W. R. (2015). The Interplay between Wnt Mediated Expansion and Negative Regulation of Growth Promotes Robust Intestinal Crypt Structure and Homeostasis. *PLoS Comput Biol, 11*(8), e1004285. doi:10.1371/journal.pcbi.1004285

E, J., Xing, J., Gong, H., He, J., & Zhang, W. (2015). Combine MEK inhibition with PI3K/mTOR inhibition exert inhibitory tumor growth effect on KRAS and PIK3CA mutation CRC xenografts due to reduced expression of VEGF and matrix metallopeptidase-9. *Tumour Biol, 36*(2), 1091-1097. doi:10.1007/s13277-014-2667-5

Ebisuya, M., Kondoh, K., & Nishida, E. (2005). The duration, magnitude and compartmentalization of ERK MAP kinase activity: mechanisms for providing signaling specificity. *J Cell Sci, 118*(Pt 14), 2997-3002. doi:10.1242/jcs.02505

el Marjou, F., Janssen, K. P., Chang, B. H., Li, M., Hindie, V., Chan, L., . . . Robine, S. (2004). Tissue-specific and inducible Cre-mediated recombination in the gut epithelium. *Genesis, 39*(3), 186-193. doi:10.1002/gene.20042

Eser, S., Reiff, N., Messer, M., Seidler, B., Gottschalk, K., Dobler, M., . . . Saur, D. (2013). Selective requirement of PI3K/PDK1 signaling for Kras oncogene-driven pancreatic cell plasticity and cancer. *Cancer Cell, 23*(3), 406-420. doi:10.1016/j.ccr.2013.01.023

Fernandes, M. S., Sanches, J. M., & Seruca, R. (2018). Targeting the PI3K Signalling as a Therapeutic Strategy in Colorectal Cancer. *Adv Exp Med Biol, 1110*, 35-53. doi:10.1007/978-3-030-02771-1_4

Fruman, D. A., Chiu, H., Hopkins, B. D., Bagrodia, S., Cantley, L. C., & Abraham, R. T. (2017). The PI3K Pathway in Human Disease. *Cell, 170*(4), 605-635. doi:10.1016/j.cell.2017.07.029

Gagliardi, P. A., di Blasio, L., & Primo, L. (2015). PDK1: A signaling hub for cell migration and tumor invasion. *Biochim Biophys Acta, 1856*(2), 178-188. doi:10.1016/j.bbcan.2015.07.003

Gagliardi, P. A., di Blasio, L., Puliafito, A., Seano, G., Sessa, R., Chianale, F., . . . Primo, L. (2014). PDK1-mediated activation of MRCKalpha regulates

directional cell migration and lamellipodia retraction. *J Cell Biol, 206*(3), 415-434. doi:10.1083/jcb.201312090

Gagliardi, P. A., Puliafito, A., & Primo, L. (2018). PDK1: At the crossroad of cancer signaling pathways. *Semin Cancer Biol, 48*, 27-35. doi:10.1016/j.semcancer.2017.04.014

Hadac, J. N., Leystra, A. A., Paul Olson, T. J., Maher, M. E., Payne, S. N., Yueh, A. E., . . . Deming, D. A. (2015). Colon Tumors with the Simultaneous Induction of Driver Mutations in APC, KRAS, and PIK3CA Still Progress through the Adenoma-to-carcinoma Sequence. *Cancer Prev Res (Phila), 8*(10), 952-961. doi:10.1158/1940-6207.CAPR-15-0003

Half, E., Bercovich, D., & Rozen, P. (2009). Familial adenomatous polyposis. *Orphanet J Rare Dis, 4*, 22. doi:10.1186/1750-1172-4-22

Hara, K., Saito, T., Hayashi, T., Yimit, A., Takahashi, M., Mitani, K., . . . Yao, T. (2015). A mutation spectrum that includes GNAS, KRAS and TP53 may be shared by mucinous neoplasms of the appendix. *Pathol Res Pract, 211*(9), 657-664. doi:10.1016/j.prp.2015.06.004

Hingorani, S. R., Petricoin, E. F., Maitra, A., Rajapakse, V., King, C., Jacobetz, M. A., . . . Tuveson, D. A. (2003). Preinvasive and invasive ductal pancreatic cancer and its early detection in the mouse. *Cancer Cell, 4*(6), 437-450. doi:10.1016/s1535-6108(03)00309-x

Hong, S. N. (2018). Genetic and epigenetic alterations of colorectal cancer. *Intest Res, 16*(3), 327-337. doi:10.5217/ir.2018.16.3.327

Kemmochi, T., Egawa, T., Mihara, K., Ito, Y., Ohkubo, Y., Mori, T., . . . Yamamuro, W. (2013). [Neoadjuvant chemotherapy with capecitabine plus oxaliplatin and bevacizumab for the treatment of patients with resectable metastatic colorectal cancer]. *Gan To Kagaku Ryoho, 40*(12), 1629-1631.

King, C. C., Gardiner, E. M., Zenke, F. T., Bohl, B. P., Newton, A. C., Hemmings, B. A., & Bokoch, G. M. (2000). p21-activated kinase (PAK1) is phosphorylated and activated by 3-phosphoinositide-dependent kinase-1 (PDK1). *J Biol Chem, 275*(52), 41201-41209. doi:10.1074/jbc.M006553200

Kobayashi, T., Deak, M., Morrice, N., & Cohen, P. (1999). Characterization of the structure and regulation of two novel isoforms of serum- and glucocorticoid-induced protein kinase. *Biochem J, 344 Pt 1*, 189-197.

Komander, D., Fairservice, A., Deak, M., Kular, G. S., Prescott, A. R., Peter Downes, C., . . . van Aalten, D. M. (2004). Structural insights into the regulation of PDK1 by phosphoinositides and inositol phosphates. *EMBO J, 23*(20), 3918-3928. doi:10.1038/sj.emboj.7600379

Koo, B. K., Stange, D. E., Sato, T., Karthaus, W., Farin, H. F., Huch, M., . . . Clevers, H. (2011). Controlled gene expression in primary Lgr5 organoid cultures. *Nat Methods, 9*(1), 81-83. doi:10.1038/nmeth.1802

Kuipers, E. J., Grady, W. M., Lieberman, D., Seufferlein, T., Sung, J. J., Boelens, P. G., . . . Watanabe, T. (2015). Colorectal cancer. *Nat Rev Dis Primers, 1*, 15065. doi:10.1038/nrdp.2015.65

Lawlor, M. A., Mora, A., Ashby, P. R., Williams, M. R., Murray-Tait, V., Malone, L., . . . Alessi, D. R. (2002). Essential role of PDK1 in regulating cell size and development in mice. *EMBO J, 21*(14), 3728-3738. doi:10.1093/emboj/cdf387

Lemmon, M. A., & Schlessinger, J. (2010). Cell signaling by receptor tyrosine kinases. *Cell, 141*(7), 1117-1134. doi:10.1016/j.cell.2010.06.011

Leoz, M. L., Carballal, S., Moreira, L., Ocana, T., & Balaguer, F. (2015). The genetic basis of familial adenomatous polyposis and its implications for clinical practice and risk management. *Appl Clin Genet, 8*, 95-107. doi:10.2147/TACG.S51484

Leystra, A. A., Deming, D. A., Zahm, C. D., Farhoud, M., Olson, T. J., Hadac, J. N., . . . Halberg, R. B. (2012). Mice expressing activated PI3K rapidly develop advanced colon cancer. *Cancer Res, 72*(12), 2931-2936. doi:10.1158/0008-5472.CAN-11-4097

Li, C., Niu, Y., Zheng, H., Shan, C., Chen, Q., Yang, Z., . . . Gao, H. (2019). Metabolic remodeling of cardiomyocytes identified in phosphoinositide-dependent kinase 1-deficient mice. *Biochem J, 476*(13), 1943-1954. doi:10.1042/BCJ20190105

Li, R., Pourpak, A., & Morris, S. W. (2009). Inhibition of the insulin-like growth factor-1 receptor (IGF1R) tyrosine kinase as a novel cancer therapy approach. *J Med Chem, 52*(16), 4981-5004. doi:10.1021/jm9002395

Lu, Z., Cox-Hipkin, M. A., Windsor, W. T., & Boyapati, A. (2010). 3-phosphoinositide-dependent protein kinase-1 regulates proliferation and survival of cancer cells with an activated mitogen-activated protein kinase pathway. *Mol Cancer Res, 8*(3), 421-432. doi:10.1158/1541-7786.MCR-09-0179

Luo, J., Field, S. J., Lee, J. Y., Engelman, J. A., & Cantley, L. C. (2005). The p85 regulatory subunit of phosphoinositide 3-kinase down-regulates IRS-1 signaling via the formation of a sequestration complex. *J Cell Biol, 170*(3), 455-464. doi:10.1083/jcb.200503088

Manning, B. D. (2004). Balancing Akt with S6K: implications for both metabolic diseases and tumorigenesis. *J Cell Biol, 167*(3), 399-403. doi:10.1083/jcb.200408161

Mendoza, M. C., Er, E. E., & Blenis, J. (2011). The Ras-ERK and PI3K-mTOR pathways: cross-talk and compensation. *Trends Biochem Sci, 36*(6), 320-328. doi:10.1016/j.tibs.2011.03.006

Montagner, A., Yart, A., Dance, M., Perret, B., Salles, J. P., & Raynal, P. (2005). A novel role for Gab1 and SHP2 in epidermal growth factor-induced Ras activation. *J Biol Chem, 280*(7), 5350-5360. doi:10.1074/jbc.M410012200

Mora, A., Komander, D., van Aalten, D. M., & Alessi, D. R. (2004). PDK1, the master regulator of AGC kinase signal transduction. *Semin Cell Dev Biol, 15*(2), 161-170. doi:10.1016/j.semcdb.2003.12.022

Mullis, K., Faloona, F., Scharf, S., Saiki, R., Horn, G., & Erlich, H. (1992). Specific enzymatic amplification of DNA in vitro: the polymerase chain reaction. 1986. *Biotechnology, 24*, 17-27.

Murillo, M. M., Zelenay, S., Nye, E., Castellano, E., Lassailly, F., Stamp, G., & Downward, J. (2014). RAS interaction with PI3K p110alpha is required for

tumor-induced angiogenesis. *J Clin Invest, 124*(8), 3601-3611. doi:10.1172/JCI74134

Najafov, A., Sommer, E. M., Axten, J. M., Deyoung, M. P., & Alessi, D. R. (2011). Characterization of GSK2334470, a novel and highly specific inhibitor of PDK1. *Biochem J, 433*(2), 357-369. doi:10.1042/BJ20101732

Narayanankutty, A. (2019). PI3K/ Akt/ mTOR Pathway as a Therapeutic Target for Colorectal Cancer: A Review of Preclinical and Clinical Evidence. *Curr Drug Targets, 20*(12), 1217-1226. doi:10.2174/1389450120666190618123846

Niba, E. T., Nagaya, H., Kanno, T., Tsuchiya, A., Gotoh, A., Tabata, C., . . . Nishizaki, T. (2013). Crosstalk between PI3 kinase/PDK1/Akt/Rac1 and Ras/Raf/MEK/ERK pathways downstream PDGF receptor. *Cell Physiol Biochem, 31*(6), 905-913. doi:10.1159/000350108

Pal, D., Outram, S. P., & Basu, A. (2013). Upregulation of PKCeta by PKCepsilon and PDK1 involves two distinct mechanisms and promotes breast cancer cell survival. *Biochim Biophys Acta, 1830*(8), 4040-4045. doi:10.1016/j.bbagen.2013.03.028

Panarelli, N. C., & Yantiss, R. K. (2011). Mucinous neoplasms of the appendix and peritoneum. *Arch Pathol Lab Med, 135*(10), 1261-1268. doi:10.5858/arpa.2011-0034-RA

Patil, D. T., Shadrach, B. L., Rybicki, L. A., Leach, B. H., & Pai, R. K. (2012). Proximal colon cancers and the serrated pathway: a systematic analysis of precursor histology and BRAF mutation status. *Mod Pathol, 25*(10), 1423-1431. doi:10.1038/modpathol.2012.98

Petrioli, R., Francini, E., Cherri, S., Torre, P., Fiaschi, A. I., Miano, S. T., . . . Francini, G. (2018). Capecitabine Plus Oxaliplatin and Bevacizumab, Followed by Maintenance Treatment With Capecitabine and Bevacizumab for Patients Aged > 75 Years With Metastatic Colorectal Cancer. *Clin Colorectal Cancer, 17*(4), e663-e669. doi:10.1016/j.clcc.2018.07.002

Rad, R., Cadinanos, J., Rad, L., Varela, I., Strong, A., Kriegl, L., . . . Bradley, A. (2013). A genetic progression model of Braf(V600E)-induced intestinal tumorigenesis reveals targets for therapeutic intervention. *Cancer Cell, 24*(1), 15-29. doi:10.1016/j.ccr.2013.05.014

Sarbassov, D. D., Guertin, D. A., Ali, S. M., & Sabatini, D. M. (2005). Phosphorylation and regulation of Akt/PKB by the rictor-mTOR complex. *Science, 307*(5712), 1098-1101. doi:10.1126/science.1106148

Sathe, A., Chalaud, G., Oppolzer, I., Wong, K. Y., von Busch, M., Schmid, S. C., . . . Nawroth, R. (2018). Parallel PI3K, AKT and mTOR inhibition is required to control feedback loops that limit tumor therapy. *PLoS One, 13*(1), e0190854. doi:10.1371/journal.pone.0190854

Sato, H., Yamamoto, H., Sakaguchi, M., Shien, K., Tomida, S., Shien, T., . . . Toyooka, S. (2018). Combined inhibition of MEK and PI3K pathways overcomes acquired resistance to EGFR-TKIs in non-small cell lung cancer. *Cancer Sci, 109*(10), 3183-3196. doi:10.1111/cas.13763

Sato, T., van Es, J. H., Snippert, H. J., Stange, D. E., Vries, R. G., van den Born, M., . . . Clevers, H. (2011). Paneth cells constitute the niche for Lgr5 stem cells in intestinal crypts. *Nature, 469*(7330), 415-418. doi:10.1038/nature09637

Schlessinger, J. (2000). Cell signaling by receptor tyrosine kinases. *Cell, 103*(2), 211-225. doi:10.1016/s0092-8674(00)00114-8

Schonhuber, N., Seidler, B., Schuck, K., Veltkamp, C., Schachtler, C., Zukowska, M., . . . Saur, D. (2014). A next-generation dual-recombinase system for time- and host-specific targeting of pancreatic cancer. *Nat Med, 20*(11), 1340-1347. doi:10.1038/nm.3646

Shafik, A., El-Sibai, O., & Ahmed, A. (2001). Study of the mechanism underlying the difference in motility between the large and small intestine: the "single" and "multiple" pacemaker theory. *Front Biosci, 6*, B1-5. doi:10.2741/a584

Sheppard, M. S., & Sterns, E. E. (1975). The difference in the clearance of interstitial albumin by the lymphatics from the stomach and the small and large intestine. *Surg Gynecol Obstet, 140*(3), 405-408.

Shi, Y., Zhang, W., Ye, Y., Cheng, Y., Han, L., Liu, P., . . . Yu, J. (2018). Benefit of everolimus as a monotherapy for a refractory breast cancer patient bearing multiple genetic mutations in the PI3K/AKT/mTOR signaling pathway. *Cancer Biol Med, 15*(3), 314-321. doi:10.20892/j.issn.2095-3941.2017.0188

Siegel, R. L., Miller, K. D., Goding Sauer, A., Fedewa, S. A., Butterly, L. F., Anderson, J. C., . . . Jemal, A. (2020). Colorectal cancer statistics, 2020. *CA Cancer J Clin, 70*(3), 145-164. doi:10.3322/caac.21601

Slattery, M. L., Mullany, L. E., Sakoda, L. C., Wolff, R. K., Stevens, J. R., Samowitz, W. S., & Herrick, J. S. (2018). The PI3K/AKT signaling pathway: Associations of miRNAs with dysregulated gene expression in colorectal cancer. *Mol Carcinog, 57*(2), 243-261. doi:10.1002/mc.22752

Smith, R. J., Rao-Bhatia, A., & Kim, T. H. (2017). Signaling and epigenetic mechanisms of intestinal stem cells and progenitors: insight into crypt homeostasis, plasticity, and niches. *Wiley Interdiscip Rev Dev Biol, 6*(5). doi:10.1002/wdev.281

Snippert, H. J., van der Flier, L. G., Sato, T., van Es, J. H., van den Born, M., Kroon-Veenboer, C., . . . Clevers, H. (2010). Intestinal crypt homeostasis results from neutral competition between symmetrically dividing Lgr5 stem cells. *Cell, 143*(1), 134-144. doi:10.1016/j.cell.2010.09.016

Stastna, M., Janeckova, L., Hrckulak, D., Kriz, V., & Korinek, V. (2019). Human Colorectal Cancer from the Perspective of Mouse Models. *Genes (Basel), 10*(10). doi:10.3390/genes10100788

Steelman, L. S., Chappell, W. H., Abrams, S. L., Kempf, R. C., Long, J., Laidler, P., . . . McCubrey, J. A. (2011). Roles of the Raf/MEK/ERK and PI3K/PTEN/Akt/mTOR pathways in controlling growth and sensitivity to therapy-implications for cancer and aging. *Aging (Albany NY), 3*(3), 192-222. doi:10.18632/aging.100296

Stokoe, D., Stephens, L. R., Copeland, T., Gaffney, P. R., Reese, C. B., Painter, G. F., . . . Hawkins, P. T. (1997). Dual role of phosphatidylinositol-3,4,5-

trisphosphate in the activation of protein kinase B. *Science, 277*(5325), 567-570. doi:10.1126/science.277.5325.567

Tan, J., Li, Z., Lee, P. L., Guan, P., Aau, M. Y., Lee, S. T., . . . Yu, Q. (2013). PDK1 signaling toward PLK1-MYC activation confers oncogenic transformation, tumor-initiating cell activation, and resistance to mTOR-targeted therapy. *Cancer Discov, 3*(10), 1156-1171. doi:10.1158/2159-8290.CD-12-0595

Tawaramoto, K., Kotani, K., Hashiramoto, M., Kanda, Y., Nagare, T., Sakaue, H., . . . Kaku, K. (2012). Ablation of 3-phosphoinositide-dependent protein kinase 1 (PDK1) in vascular endothelial cells enhances insulin sensitivity by reducing visceral fat and suppressing angiogenesis. *Mol Endocrinol, 26*(1), 95-109. doi:10.1210/me.2010-0412

Testa, U., Pelosi, E., & Castelli, G. (2018). Colorectal cancer: genetic abnormalities, tumor progression, tumor heterogeneity, clonal evolution and tumor-initiating cells. *Med Sci (Basel), 6*(2). doi:10.3390/medsci6020031

Tirumani, S. H., Fraser-Hill, M., Auer, R., Shabana, W., Walsh, C., Lee, F., & Ryan, J. G. (2013). Mucinous neoplasms of the appendix: a current comprehensive clinicopathologic and imaging review. *Cancer Imaging, 13*, 14-25. doi:10.1102/1470-7330.2013.0003

Trapnell, C., Pachter, L., & Salzberg, S. L. (2009). TopHat: discovering splice junctions with RNA-Seq. *Bioinformatics, 25*(9), 1105-1111. doi:10.1093/bioinformatics/btp120

Turke, A. B., Song, Y., Costa, C., Cook, R., Arteaga, C. L., Asara, J. M., & Engelman, J. A. (2012). MEK inhibition leads to PI3K/AKT activation by relieving a negative feedback on ERBB receptors. *Cancer Res, 72*(13), 3228-3237. doi:10.1158/0008-5472.CAN-11-3747

Tzanikou, E., Markou, A., Politaki, E., Koutsopoulos, A., Psyrri, A., Mavroudis, D., . . . Lianidou, E. (2019). PIK3CA hotspot mutations in circulating tumor cells and paired circulating tumor DNA in breast cancer: a direct comparison study. *Mol Oncol, 13*(12), 2515-2530. doi:10.1002/1878-0261.12540

Velho, S., Moutinho, C., Cirnes, L., Albuquerque, C., Hamelin, R., Schmitt, F., . . . Seruca, R. (2008). BRAF, KRAS and PIK3CA mutations in colorectal serrated polyps and cancer: primary or secondary genetic events in colorectal carcinogenesis? *BMC Cancer, 8*, 255. doi:10.1186/1471-2407-8-255

Wang, J., Li, R., He, Y., Yi, Y., Wu, H., & Liang, Z. (2020). Next-generation sequencing reveals heterogeneous genetic alterations in key signaling pathways of mismatch repair deficient colorectal carcinomas. *Mod Pathol*. doi:10.1038/s41379-020-0612-2

Wang, J., Yuan, Y., Zhou, Y., Guo, L., Zhang, L., Kuai, X., . . . He, F. (2008). Protein interaction data set highlighted with human Ras-MAPK/PI3K signaling pathways. *J Proteome Res, 7*(9), 3879-3889. doi:10.1021/pr8001645

Wick, M. J., Ramos, F. J., Chen, H., Quon, M. J., Dong, L. Q., & Liu, F. (2003). Mouse 3-phosphoinositide-dependent protein kinase-1 undergoes dimerization and trans-phosphorylation in the activation loop. *J Biol Chem, 278*(44), 42913-42919. doi:10.1074/jbc.M304172200

Winter, J. N., Jefferson, L. S., & Kimball, S. R. (2011). ERK and Akt signaling pathways function through parallel mechanisms to promote mTORC1 signaling. *Am J Physiol Cell Physiol, 300*(5), C1172-1180. doi:10.1152/ajpcell.00504.2010

Xie, Y. H., Chen, Y. X., & Fang, J. Y. (2020). Comprehensive review of targeted therapy for colorectal cancer. *Signal Transduct Target Ther, 5*(1), 22. doi:10.1038/s41392-020-0116-z

Yamane, L., Scapulatempo-Neto, C., Reis, R. M., & Guimaraes, D. P. (2014). Serrated pathway in colorectal carcinogenesis. *World J Gastroenterol, 20*(10), 2634-2640. doi:10.3748/wjg.v20.i10.2634

Yang, J. Y., Zong, C. S., Xia, W., Yamaguchi, H., Ding, Q., Xie, X., . . . Hung, M. C. (2008). ERK promotes tumorigenesis by inhibiting FOXO3a via MDM2-mediated degradation. *Nat Cell Biol, 10*(2), 138-148. doi:10.1038/ncb1676

Ye, Q., Cai, W., Zheng, Y., Evers, B. M., & She, Q. B. (2014). ERK and AKT signaling cooperate to translationally regulate survivin expression for metastatic progression of colorectal cancer. *Oncogene, 33*(14), 1828-1839. doi:10.1038/onc.2013.122

Yeates, L. C., Gallegos, A., Kozikowski, A. P., & Powis, G. (1999). Down regulation of the expression of the p110, p85 and p55 subunits of phosphatidylinositol 3-kinase during colon cancer cell anchorage-independent growth. *Anticancer Res, 19*(5B), 4171-4176.

Yu, X. R., Mao, J., Tang, W., Meng, X. Y., Tian, Y., & Du, Z. L. (2020). Low-grade appendiceal mucinous neoplasms confined to the appendix: clinical manifestations and CT findings. *J Investig Med, 68*(1), 75-81. doi:10.1136/jim-2018-000975

Zhang, J., Roberts, T. M., & Shivdasani, R. A. (2011). Targeting PI3K signaling as a therapeutic approach for colorectal cancer. *Gastroenterology, 141*(1), 50-61. doi:10.1053/j.gastro.2011.05.010

Zhang, S. Q., Tsiaras, W. G., Araki, T., Wen, G., Minichiello, L., Klein, R., & Neel, B. G. (2002). Receptor-specific regulation of phosphatidylinositol 3'-kinase activation by the protein tyrosine phosphatase Shp2. *Mol Cell Biol, 22*(12), 4062-4072. doi:10.1128/mcb.22.12.4062-4072.2002

Zheng, W. H., & Quirion, R. (2006). Insulin-like growth factor-1 (IGF-1) induces the activation/phosphorylation of Akt kinase and cAMP response element-binding protein (CREB) by activating different signaling pathways in PC12 cells. *BMC Neurosci, 7*, 51. doi:10.1186/1471-2202-7-51

Ziemba, B. P., Burke, J. E., Masson, G., Williams, R. L., & Falke, J. J. (2016). Regulation of PI3K by PKC and MARCKS: Single-Molecule Analysis of a Reconstituted Signaling Pathway. *Biophys J, 110*(8), 1811-1825. doi:10.1016/j.bpj.2016.03.001